Proton acceleration in thermonuclear nova explosions revealed by gamma rays

Gamma rays reveal proton acceleration in thermonuclear novae explosions

MAGIC Collaboration et al.,*†

†The full list of authors and their affiliations is included in the supplementary material
*corresponding authors(contact.magic@mpp.mpg.de): J. Sitarek, R. López-Coto, D. Green, A. López-Oramas

Classical novae are cataclysmic binary star systems in which the matter of a companion star is accreted on a white dwarf (WD) [1, 2]. Accumulation of the matter in a layer eventually causes a thermonuclear explosion on the surface of the WD [3], brightening the WD to $\sim 10^5$ solar luminosities and triggering ejection of the accumulated matter. They provide extreme conditions required to accelerate particles, electrons or protons, to high energies. Here we present the detection of gamma rays by the MAGIC telescopes from the 2021 outburst of RS Ophiuchi (RS Oph), a recurrent symbiotic nova, that allowed us, for the first time, to accurately characterize the emission from a nova in the 60 GeV to 250 GeV energy range. The theoretical interpretation of the combined *Fermi*-LAT and MAGIC data suggests that protons are accelerated to hundreds of GeV in the nova shock. Such protons should create bubbles of enhanced Cosmic Ray density up to about 13 pc from the recurrent novae.

A symbiotic nova can be formed when the companion star of the WD is a red giant (RG) [4]. The ejecta of symbiotic novae expand within the dense wind of the RG companion. Novae outbursts usually last from weeks to months. While they are expected to repeat hundreds of times [5, 6], for most of them the interval between subsequent events can be hundreds of thousand years. However, a subclass of objects called Recurrent Novae (RNe) allows one to observe such repeated outbursts over a human lifespan [7]. In our Galaxy, ten such objects are known in which the repetition of bursts has been seen within a century [6]. According to [8] for the symbiotic nova to become recurrent, its WD must be massive ($\geq$1.1 $M_\odot$).

Novae have been deeply studied in the optical and X-ray ranges for decades[9], but only recently they have been shown as emitters of high-energy gamma-ray radiation: first in the case of symbiotic novae [10] and soon after with classical novae [11]. Though this clearly indicates that charged particles are accelerated to high energies in novae, their nature and radiation mechanism are not yet clear. In order to understand the acceleration mechanism of high-energy particles, it is crucial to measure the maximum energies of the emitted radiation. Until recently, all spectra of gamma-ray novae have been measured only up to 6 – 10 GeV range [11] with no hint of emission at higher energies [12, 13].

RS Oph is a recurrent symbiotic nova which displays major outbursts every 15-20 years [14]. The latest outburst, in August 2021, was promptly reported in optical [15] and high-energy (HE, $100\,\mathrm{MeV} < E < 10\,\mathrm{GeV}$) gamma rays by *Fermi*-LAT [16]. Following these alerts, MAGIC began observations of RS Oph as part of its nova follow-up program [13], on August 09, 2021 at 22:27 UT, i.e., about 1 day after the first optical and GeV detections. In parallel, the H.E.S.S. collaboration announced very-high-energy (VHE, $\gtrsim 100\,\mathrm{GeV}$) gamma rays from RS Oph [17]. The MAGIC observations reveal VHE emission contemporaneous to the *Fermi*-LAT and optical maxima, and a decrease below the VHE detection limit two weeks later (see Fig. 1). Details of the analysis can be found in Section B.1. The first four days of MAGIC observations (August 09-12) yield a VHE signal with a significance of $13.2\,\sigma$, spanning from 60 GeV to 250 GeV, well fitted by a single power-law ($\chi^2/N_{dof} = 5.9/5$). Daily spectra are reconstructed (see Sections B.1 and C.5) allowing us to track the evolution of the outburst.

The contemporaneous gamma-ray spectrum measured by *Fermi*-LAT and MAGIC can be described as a single, smooth component spanning from 50 MeV to 250 GeV. Intriguingly, while the GeV emission subsides with a halving time scale of ~ 2.2 days (see also Section B.2), the flux measured by MAGIC over the first four days is consistent with being constant ($\chi^2/\mathrm{N_{dof}} = 2.9/3$). This suggests a migration of the gamma-ray emission towards higher energies, in line with an increase of the maximum energies of the parent particles. RS Oph is the gamma-ray nova with the highest flux and energy output to date, as shown by the comparison with the other Fermi-LAT detected novae presented in Section D. Therefore, the non-detection of previous novae at VHE range [12, 13] might be explained by the lack of sensitivity to dimmer eruptions, without the need to invoke any fundamental difference in the spectral energy distribution of RS Oph.

The conditions in novae are favourable for the acceleration and subsequent emission of radiation by both electrons and protons [11]. The expanding ejecta of a nova interacting with the interstellar medium (filled also with the dense RG wind in the case of symbiotic novae) will result in the formation of a shock wave. Moreover, the fast wind, induced by the nuclear burning on the surface of the WD, will catch up with the ejecta, causing an additional internal shock [18]. Recently, a correlation between optical and gamma-ray emission

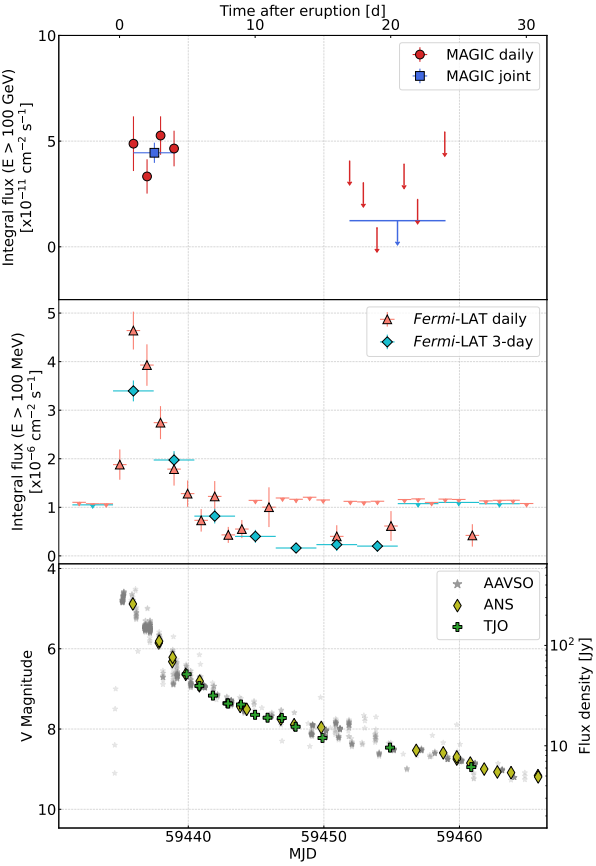

Fig. 1 Multiwavelength light curve in the VHE (MAGIC, top panel), high-energy (*Fermi*-LAT, middle panel) and optical (TJO, ANS, and AAVSO, bottom panel) bands

has confirmed that a substantial part of the novae explosion's power goes into shocks [19]. In such shocks, energetic electrons and protons can be produced (see Fig. 2). Gamma-ray emission can arise from photosphere thermal radiation up-scattered to the gamma-ray energy range by relativistic electrons via inverse Compton scattering. Alternatively, the ambient matter (nova ejecta and RG wind) can act as a target for hadronic interaction of protons or Bremsstrahlung radiation of electrons [11]. The maximum energies of high-energy particles will depend on the efficiency of the acceleration mechanism, duration of the nova, and the cooling energy losses (see Section C.1). Protons experience only

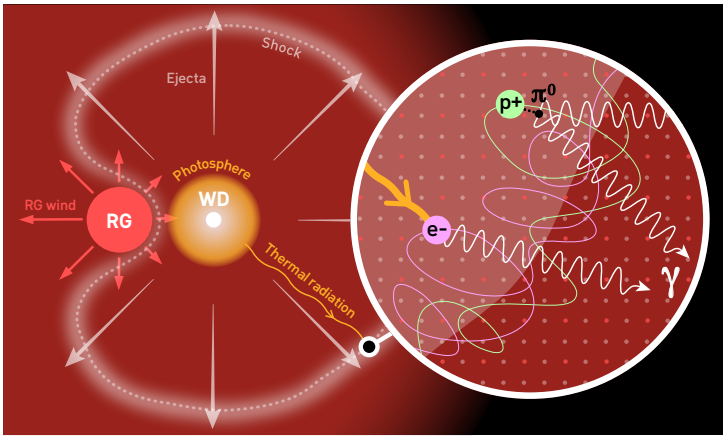

Fig. 2 Schematic representation of RS Oph during an outburst. A photosphere (yellow circle) surrounds the White Dwarf (WD, white small circle). Its companion star, a red giant (RG, red circle) emits a slow wind (red arrows). Ejecta of the nova explosion (gray arrows) propagate into the surrounding medium causing a shock wave encompassing the binary system (gray dashed line). In the shock wave, energetic electrons and protons (magenta and green wavy lines, respectively) are trapped by a magnetic field and accelerated. Gamma rays (white arrows) are produced by either electrons scattering the thermal radiation of the photosphere (yellow arrow) or by protons interacting with the surrounding matter (gray and red dots).

mild cooling by proton-proton interactions with time scale of $t_{pp} = 21(n_p/6 \times 10^8\,\mathrm{cm}^{-3})^{-1}$ [days], where n_p is the number density of the target material. Electrons in nova shocks suffer stronger inverse Compton energy losses with $t_{IC} = 4.4 \times 10^{-3}(E/300\,\mathrm{GeV})^{-1})[1 + 10(E/300\,\mathrm{GeV})]^{1.5}$ [days]. Therefore, the production of high energy photons via leptonic mechanisms is much more demanding on the acceleration processes efficiency than for proton models. The simultaneous acceleration of both types of particles (but reaching different energies) has also been proposed [13, 20]. We estimate that Bremsstrahlung is negligible with respect to inverse Compton component for the parameters of RS Oph (see Section C).

Based on the optical observations of RS Oph during the 2021 outburst, and the derived parameters from previous outbursts of the source, we model the gamma-ray emission with the injection of a population of relativistic electrons or protons (see Section C). The *Fermi*-LAT and MAGIC measurement can be well described ($\chi^2/\mathrm{N_{dof}} = 13.1/12$, p-value $= 0.36$) with the proton-only model (see left panel of Fig. 3). The fit yields a canonical power-law spectrum with an index ~ -2 and an exponential cut-off, corresponding to the maximum energies achieved in the acceleration. The day-by-day modeling shows evidence that the energy cut-off of protons increases with time (see Section C.5). This goes in line with absence of spectral signatures from cooling terms. The associated neutrino emission is not expected to be detected by the current experiments (see Section C.4).

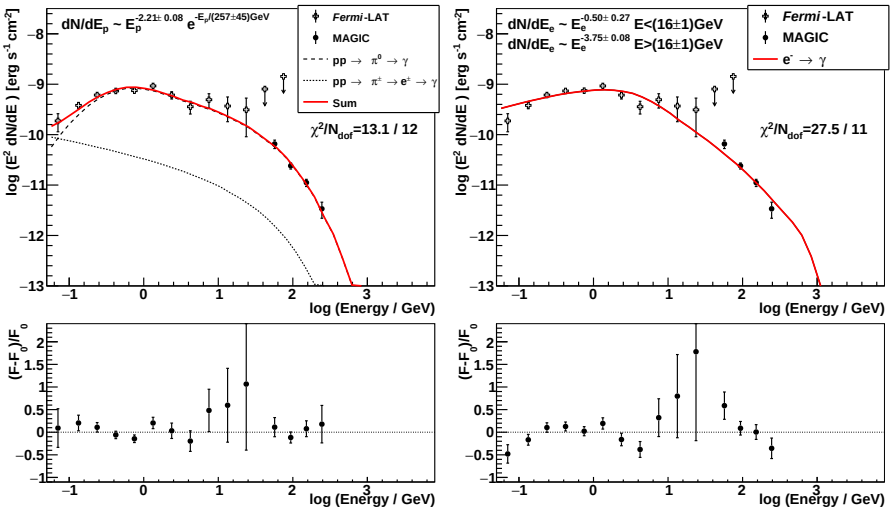

Fig. 3 Gamma-ray spectrum of RS Oph observed with *Fermi*-LAT (empty crosses) and MAGIC (filled circles), modeled within hadronic (left panel) or leptonic (right panel) scenario. The dashed line shows the gamma rays from the π^0 decay and the dotted line shows the inverse Compton contribution of the secondary $e^{\pm}$ pairs produced in hadronic interactions. dN/dE_p and dN/dE_e report the shape of the proton and electron energy distributions obtained from the fit. The bottom panel shows the fit residuals.

In contrast, it is difficult to explain the shape of the curvature of the measured spectrum between 50 MeV and 250 GeV with leptonic processes. The leptonic model requires injection of particles that already contain a strong break (change of particles index by 3.25 ± 0.28) in the electron energy distribution (see Fig. 3, right panel). Since the break must already be present in the injection spectrum of particles, it cannot be explained by the cooling. In addition, despite a more complicated particle injection model, the description of the gamma-ray emission in the electron scenario is significantly worse ($\chi^2/\mathrm{N_{dof}} = 27.5/11$, p-value $= 3.9 \times 10^{-3}$) than in the case of protons, as can be seen in Fig. 3. The relative likelihood of the electron model with respect to the proton model for ΔAIC= 15.3, as defined within the Akaike information criterion framework [21], which is normally used for comparison of non-nested models, is 4.7×10^{-4}.

Despite their intense emission of gamma rays, accelerated protons will eventually escape the nova shock carrying away most of their obtained energy. Such protons can contribute to the Galactic Cosmic Rays (CR), which are expected to be produced mainly in supernova remnants [22]. The measurement of the proton spectrum required to explain the gamma-ray emission of RS Oph can be used to put estimates on novae contribution to CR. Using the CR energetics derived for RS Oph ($\sim 4.4 \times 10^{43}$ erg, see Section C.2), a rate of 100 novae per year would lead to about 0.2% of the CR energy contribution from supernovae, which are more rare than novae (~ 2 per century) but much more energetic ($\sim 10^{50}$ erg). Despite the small contribution to the overall CR sea, a

nova would significantly increase the CR density in its close environment. The energy density of the nova dominates over that of the average CR energy density in the Milky Way ($\sim$1 eV/cm^3) in a region of radius $\sim$0.5 pc, comparable to a distance to the nearest star in our Galaxy. In the special case of recurrent novae, protons accelerated in $\sim 10^4$ subsequent outbursts [23] will accumulate in a $\sim$ 13 pc bubble with enhanced CR density (see Section C.2.1).

The detection of gamma rays reaching 250 GeV from a symbiotic nova allowed us to obtain a deep physical insight on the population of relativistic particles accelerated by such objects. The modeling of the gamma-ray spectrum strongly favors the explanation of the emission via the acceleration of protons in a nova shock. Evidence towards the proton acceleration is based on: (i) the inferred shape of the energy distribution of injected particles, (ii) the better statistical description of the gamma-ray spectral energy distribution by the proton model, (iii) the obtained evidence of the increase of the particle maximum energies over time, consistent with lack of strong cooling. The protons in the nova shock undergo slow cooling, therefore they will be eventually able to escape the shock, carrying away a significant fraction of energy. Such protons will add to the Galactic cosmic ray budget, however primarily in the close neighborhood of novae.

The observation of the August 2021 outburst of RS Oph introduces a new class of sources as VHE gamma-ray emitter: (symbiotic) novae. RS Oph is a symbiotic nova, the same class of objects as V407 Cyg, the first nova detected in the GeV range by *Fermi*-LAT. While we now know that classical novae are also GeV emitters, it is still to be seen if the detection of RS Oph emitting in VHE gamma-ray range is due to its symbiotic nature, or just the first sign of such emission from a broader class of classical novae. The comparison of gamma-ray measurements in GeV and VHE gamma-ray range with previous *Fermi*-LAT novae does not reveal any peculiarity in the emission of RS Oph, except for its brightness. Therefore, it is likely that future, more sensitive VHE gamma-ray facilities will be able to provide an ample harvest of novae.

Supplementary information.
Full author list
Materials and Methods
Fig. 4 – 18
Tables 1 – 10
References (24-88)

Acknowledgments. We would like to thank the Instituto de Astrofísica de Canarias for the excellent working conditions at the Observatorio del Roque de los Muchachos in La Palma. The financial support of the German BMBF, MPG and HGF; the Italian INFN and INAF; the Swiss

National Fund SNF; the ERDF under the Spanish Ministerio de Ciencia e Innovación (MICINN) (PID2019-104114RB-C31, PID2019-104114RB-C32, PID2019-104114RB-C33, PID2019-105510GB-C31,PID2019-107847RB-C41, PID2019-107847RB-C42, PID2019-107847RB-C44, PID2019-107988GB-C22); the Indian Department of Atomic Energy; the Japanese ICRR, the University of Tokyo, JSPS, and MEXT; the Bulgarian Ministry of Education and Science, National RI Roadmap Project DO1-400/18.12.2020 and the Academy of Finland grant nr. 320045 is gratefully acknowledged. This work was also supported by the Spanish Centro de Excelencia "Severo Ochoa" (SEV-2016-0588, SEV-2017-0709, CEX2019-000920-S), the Unidad de Excelencia "María de Maeztu" (CEX2019-000918-M, MDM-2015-0509-18-2) and by the CERCA program of the Generalitat de Catalunya; by the Croatian Science Foundation (HrZZ) Project IP-2016-06-9782 and the University of Rijeka Project 13.12.1.3.02; by the DFG Collaborative Research Centers SFB823/C4 and SFB876/C3; the Polish National Research Centre grant UMO-2016/22/M/ST9/00382; and by the Brazilian MCTIC, CNPq and FAPERJ. The Joan Oró Telescope (TJO) of the Montsec Observatory (OdM) is owned by the Catalan Government and operated by the Institute for Space Studies of Catalonia (IEEC). We acknowledge with thanks the variable star observations from the AAVSO International Database contributed by observers worldwide and used in this research. We gratefully acknowledge the prompt response to the alert and the data provided by the CAOS Team. The authors would like to thank Giacomo Principe for the advice in extending the *Fermi*-LAT analysis below 100 MeV and Filippo D'Ammando for his comments on the manuscript. R.L-C.'s work was financially supported by the European Union's Horizon 2020 research and innovation program under the Marie Skłodowska-Curie grant agreement No. 754496 - FELLINI.

Declarations

Competing Interests: The authors declare that they have no competing interests.

Full author list

V. A. Acciari[1], S. Ansoldi[2,42], L. A. Antonelli[3], A. Arbet Engels[15], M. Artero[5], K. Asano[6], D. Baack[7], A. Babić[8], A. Baquero[9], U. Barres de Almeida[10], J. A. Barrio[9], I. Batković[11], J. Becerra González[1], W. Bednarek[12], L. Bellizzi[13], E. Bernardini[14], M. Bernardos[11], A. Berti[15], J. Besenrieder[15], W. Bhattacharyya[14], C. Bigongiari[3], A. Biland[4], O. Blanch[5], H. Bökenkamp[7], G. Bonnoli[16], Ž. Bošnjak[8], G. Busetto[11], R. Carosi[17], G. Ceribella[15], M. Cerruti[18], Y. Chai[15], A. Chilingarian[19], S. Cikota[8], S. M. Colak[5], E. Colombo[1], J. L. Contreras[9], J. Cortina[20], S. Covino[3], G. D'Amico[15,43], V. D'Elia[3], P. Da Vela[17,44], F. Dazzi[3], A. De Angelis[11], B. De Lotto[2], A. Del Popolo[21], M. Delfino[5,45], J. Delgado[5,45], C. Delgado Mendez[20], D. Depaoli[22], F. Di Pierro[22], L. Di Venere[23], E. Do Souto Espiñeira[5],

D. Dominis Prester[24], A. Donini[2], D. Dorner[25], M. Doro[11], D. Elsaesser[7], V. Fallah Ramazani[26,46], L. Fariña Alonso[5], A. Fattorini[7], M. V. Fonseca[9], L. Font[27], C. Fruck[15], S. Fukami[4], Y. Fukazawa[28], R. J. García López[1], M. Garczarczyk[14], S. Gasparyan[29], M. Gaug[27], N. Giglietto[23], F. Giordano[23], P. Gliwny[12], N. Godinović[30], J. G. Green[15], D. Green[15*], D. Hadasch[6], A. Hahn[15], T. Hassan[20], L. Heckmann[15], J. Herrera[1], J. Hoang[9,47], D. Hrupec[31], M. Hütten[6], T. Inada[6], K. Ishio[12], Y. Iwamura[6], I. Jiménez Martínez[20], J. Jormanainen[26], L. Jouvin[5], D. Kerszberg[5], Y. Kobayashi[6], H. Kubo[32], J. Kushida[33], A. Lamastra[3], D. Lelas[30], F. Leone[3], E. Lindfors[26], L. Linhoff[7], S. Lombardi[3], F. Longo[2,48], R. López-Coto[11*], M. López-Moya[9], A. López-Oramas[1*], S. Loporchio[23], B. Machado de Oliveira Fraga[10], C. Maggio[27], P. Majumdar[34], M. Makariev[35], M. Mallamaci[11], G. Maneva[35], M. Manganaro[24], K. Mannheim[25], L. Maraschi[3], M. Mariotti[11], M. Martínez[5], A. Mas Aguilar[9], D. Mazin[6,49], S. Menchiari[13], S. Mender[7], S. Mićanović[24], D. Miceli[2,50], T. Miener[9], J. M. Miranda[13], R. Mirzoyan[15], E. Molina[18], A. Moralejo[5], D. Morcuende[9], V. Moreno[27], E. Moretti[5], T. Nakamori[36], L. Nava[3], V. Neustroev[37], M. Nievas Rosillo[1], C. Nigro[5], K. Nilsson[26], K. Nishijima[33], K. Noda[6], S. Nozaki[32], Y. Ohtani[6], T. Oka[32], J. Otero-Santos[1], S. Paiano[3], M. Palatiello[2], D. Paneque[15], R. Paoletti[13], J. M. Paredes[18], L. Pavletić[24], P. Peñil[9], M. Persic[2,51], M. Pihet[15], P. G. Prada Moroni[17], E. Prandini[11], C. Priyadarshi[5], I. Puljak[30], W. Rhode[7], M. Ribó[18], J. Rico[5], C. Righi[3], A. Rugliancich[17], N. Sahakyan[29], T. Saito[6], S. Sakurai[6], K. Satalecka[14], F. G. Saturni[3], B. Schleicher[25], K. Schmidt[7], T. Schweizer[15], J. Sitarek[6*], I. Šnidarić[38], D. Sobczynska[12], A. Spolon[11], A. Stamerra[3], J. Strišković[31], D. Strom[15], M. Strzys[6], Y. Suda[28], T. Surić[38], M. Takahashi[6], R. Takeishi[6], F. Tavecchio[3], P. Temnikov[35], T. Terzić[24], M. Teshima[15,52], L. Tosti[39], S. Truzzi[13], A. Tutone[3], S. Ubach[27], J. van Scherpenberg[15], G. Vanzo[1], M. Vazquez Acosta[1], S. Ventura[13], V. Verguilov[35], C. F. Vigorito[22], V. Vitale[40], I. Vovk[6], M. Will[15], C. Wunderlich[13], T. Yamamoto[41], D. Zarić[30] and F. Ambrosino[53], M. Cecconi[54], G. Catanzaro[55], C. Ferrara[55], A. Frasca[55], M. Munari[55], L. Giustolisi[55], J. Alonso-Santiago[55], M. Giarrusso[56], U. Munari[57], P. Valisa[58]

[1] Instituto de Astrofísica de Canarias and Dpto. de Astrofísica, Universidad de La Laguna, E-38200, La Laguna, Tenerife, Spain,
[2] Università di Udine and INFN Trieste, I-33100 Udine, Italy,
[3] National Institute for Astrophysics (INAF), I-00136 Rome, Italy,
[4] ETH Zürich, CH-8093 Zürich, Switzerland,
[5] Institut de Física d'Altes Energies (IFAE), The Barcelona Institute of Science and Technology (BIST), E-08193 Bellaterra (Barcelona), Spain,
[6] Japanese MAGIC Group: Institute for Cosmic Ray Research (ICRR), The University of Tokyo, Kashiwa, 277-8582 Chiba, Japan,
[7] Technische Universität Dortmund, D-44221 Dortmund, Germany,
[8] Croatian MAGIC Group: University of Zagreb, Faculty of Electrical Engineering and Computing (FER), 10000 Zagreb, Croatia,

[9] IPARCOS Institute and EMFTEL Department, Universidad Complutense de Madrid, E-28040 Madrid, Spain,
[10] Centro Brasileiro de Pesquisas Físicas (CBPF), 22290-180 URCA, Rio de Janeiro (RJ), Brazil,
[11] Università di Padova and INFN, I-35131 Padova, Italy,
[12] University of Lodz, Faculty of Physics and Applied Informatics, Department of Astrophysics, 90-236 Lodz, Poland,
[13] Università di Siena and INFN Pisa, I-53100 Siena, Italy,
[14] Deutsches Elektronen-Synchrotron (DESY), D-15738 Zeuthen, Germany,
[15] Max-Planck-Institut für Physik, D-80805 München, Germany,
[16] Instituto de Astrofísica de Andalucía-CSIC, Glorieta de la Astronomía s/n, 18008, Granada, Spain,
[17] Università di Pisa and INFN Pisa, I-56126 Pisa, Italy,
[18] Universitat de Barcelona, ICCUB, IEEC-UB, E-08028 Barcelona, Spain,
[19] Armenian MAGIC Group: A. Alikhanyan National Science Laboratory, 0036 Yerevan, Armenia,
[20] Centro de Investigaciones Energéticas, Medioambientales y Tecnológicas, E-28040 Madrid, Spain,
[21] INFN MAGIC Group: INFN Sezione di Catania and Dipartimento di Fisica e Astronomia, University of Catania, I-95123 Catania, Italy,
[22] INFN MAGIC Group: INFN Sezione di Torino and Università degli Studi di Torino, I-10125 Torino, Italy,
[23] INFN MAGIC Group: INFN Sezione di Bari and Dipartimento Interateneo di Fisica dell'Università e del Politecnico di Bari, I-70125 Bari, Italy,
[24] Croatian MAGIC Group: University of Rijeka, Department of Physics, 51000 Rijeka, Croatia,
[25] Universität Würzburg, D-97074 Würzburg, Germany,
[26] Finnish MAGIC Group: Finnish Centre for Astronomy with ESO, University of Turku, FI-20014 Turku, Finland,
[27] Departament de Física, and CERES-IEEC, Universitat Autònoma de Barcelona, E-08193 Bellaterra, Spain,
[28] Japanese MAGIC Group: Physics Program, Graduate School of Advanced Science and Engineering, Hiroshima University, 739-8526 Hiroshima, Japan,
[29] Armenian MAGIC Group: ICRANet-Armenia at NAS RA, 0019 Yerevan, Armenia,
[30] Croatian MAGIC Group: University of Split, Faculty of Electrical Engineering, Mechanical Engineering and Naval Architecture (FESB), 21000 Split, Croatia,
[31] Croatian MAGIC Group: Josip Juraj Strossmayer University of Osijek, Department of Physics, 31000 Osijek, Croatia,
[32] Japanese MAGIC Group: Department of Physics, Kyoto University, 606-8502 Kyoto, Japan,
[33] Japanese MAGIC Group: Department of Physics, Tokai University, Hiratsuka, 259-1292 Kanagawa, Japan,
[34] Saha Institute of Nuclear Physics, HBNI, 1/AF Bidhannagar, Salt Lake,

Sector-1, Kolkata 700064, India,
[35] Inst. for Nucl. Research and Nucl. Energy, Bulgarian Academy of Sciences, BG-1784 Sofia, Bulgaria,
[36] Japanese MAGIC Group: Department of Physics, Yamagata University, Yamagata 990-8560, Japan,
[37] Finnish MAGIC Group: Astronomy Research Unit, University of Oulu, FI-90014 Oulu, Finland,
[38] Croatian MAGIC Group: Ruđer Bošković Institute, 10000 Zagreb, Croatia,
[39] INFN MAGIC Group: INFN Sezione di Perugia, I-06123 Perugia, Italy,
[40] INFN MAGIC Group: INFN Roma Tor Vergata, I-00133 Roma, Italy,
[41] Japanese MAGIC Group: Department of Physics, Konan University, Kobe, Hyogo 658-8501, Japan,
[42] also at International Center for Relativistic Astrophysics (ICRA), Rome, Italy,
[43] now at Department for Physics and Technology, University of Bergen, NO-5020, Norway,
[44] now at University of Innsbruck,
[45] also at Port d'Informació Científica (PIC), E-08193 Bellaterra (Barcelona), Spain,
[46] now at Ruhr-Universität Bochum, Fakultät für Physik und Astronomie, Astronomisches Institut (AIRUB), 44801 Bochum, Germany,
[47] now at Department of Astronomy, University of California Berkeley, Berkeley CA 94720,
[48] also at Dipartimento di Fisica, Università di Trieste, I-34127 Trieste, Italy,
[49] Max-Planck-Institut für Physik, D-80805 München, Germany,
[50] now at Laboratoire d'Annecy de Physique des Particules (LAPP), CNRS-IN2P3, 74941 Annecy Cedex, France,
[51] also at INAF Trieste and Dept. of Physics and Astronomy, University of Bologna, Bologna, Italy,
[52] Japanese MAGIC Group: Institute for Cosmic Ray Research (ICRR), The University of Tokyo, Kashiwa, 277-8582 Chiba, Japan
[53] INAF - Osservatorio Astrofisico di Roma, Via Frascati 33, I–00078, Monteporzio Catone (Roma) Italy,
[54] INAF - Fund. Galileo Galilei, Rambla José Ana Fernández Perez 7, 38712 Brenã Baja (La Palma), Canary Islands, Spain,
[55] INAF – Osservatorio Astrofisico di Catania, Via S. Sofia 78, 95123 Catania, Italy,
[56] INFN - Laboratori Nazionali del Sud, Via S. Sofia 62, I–95123 Catania, Italy,
[57] INAF - Osservatorio Astronomico di Padova, I-36012 Asiago (Vi), Italy,
[58] ANS Collaboration, c/o Astronomical Observatory, I-36012 Asiago (VI), Italy

Materials and Methods

A The symbiotic nova RS Oph

RS Oph is composed by a massive carbon-oxygen white dwarf (WD) [24] and a M0-2 III mass-donor RG star [25]. The orbital solution implies a WD mass of $M_{WD} = 1.2 - 1.4 M_{\odot}$ and an RG mass of $M_{RG} = 0.68 - 0.80 M_{\odot}$. Interestingly, RS Oph was pointed out as a plausible source from which GeV emission can be detected [26]. It is also a type Ia Supernova progenitor candidate [6]. The system has a period of (453.6 ± 0.4) days [27]. The system has a circular ($e \approx 0$) orbit[14, 28], however a mild eccentricity has been claimed as well ($e = 0.14 \pm 0.03$) [27]. The estimation of the wind mass loss rate of the RG in RS Oph varies between $3.7 \times 10^{-8} M_{\odot}\,\mathrm{yr}^{-1}$ [29] and $10^{-6} M_{\odot}\,\mathrm{yr}^{-1}$ [30]. An outburst was reported on August 08, 2021 (MJD $T_0 = 59434.93$) [16]. The spectroscopy measurements performed in the first few days of the nova show mild acceleration of the ejecta from $3700 - 2700\ \mathrm{km\,s^{-1}}$ at $T_0 + 0.87\,\mathrm{d}$ to $4200 - 4700\ \mathrm{km\,s^{-1}}$ at $T_0 + 2\,\mathrm{d}$ for the Hα and Hβ P Cyg lines, respectively [31, 32]. We assume an ejecta speed of $v_{sh} = 4500\,\mathrm{km\,s^{-1}}$, see Section B.4. The equipartition magnetic field derived from observations starting 20 days after the 2006 outburst is $B = 0.08 - 0.11\,\mathrm{G}$ [33], while the estimate 18.5 d after the 1985 nova onset was 0.04 G [34]. In the case of a similar recurrent nova, V1535 Sco, a value of $B = 0.13 - 0.17\,\mathrm{G}$ was measured one week after the outburst [35] and for V745 Sco 0.03 G at the distance of the shock of 4.5×10^{14} cm [36]. It should be noted that, as the shock dissipates, B declines over time.

A.1 Estimates of the RS Oph distance to Earth

The distance to RS Oph has been object of intense debate (see Table 1). Historically, a value of 1.6 kpc was estimated [37, 38] and canonically assumed. Dedicated discussions on the distance were performed in the past [39] in which a distance of 1.4 kpc was considered the most likely one. The value is however at odds with the mass accumulation rate needed for repetition period of RS Oph. Namely, at such assumed distance, the calculated blackbody radius of the secondary star must greatly underfill its Roche lobe [40].

More recently, the parallax distance to the source of (2.68 ± 0.16) kpc was provided by Gaia [41]. However, as it is discussed in [40], Gaia Data Release 2 (and Gaia Early Data Release 3) do not have reliable measures of the parallaxes for RS Oph. The issue arises due to the long-period binary orbit which makes the center of light wobble back and forth with a greater amplitude than the parallax itself, not providing a good fit to the single-star model applied in these data releases.

Using different estimates, [29] pointed out that if one argues that the RG needs to fill its Roche lobe to efficiently accrete matter onto the WD, the favored distance to the source is > 3 kpc, very likely (4.3 ± 0.7) kpc, and the earlier, lower estimates suffered from overestimated absorption along the line

Table 1 Different distances estimated for RS Oph. The distance assumed in subsequent calculations is highlighted in bold font.

Distance [kpc]	Method	Reference
1.6	H I absorption measurements	[37, 38]
$1.4^{+0.6}_{-0.2}$	Several estimations	[39]
2.45 ± 0.37	**Expansion velocity**	[42]
> 3	Requirement of RG filling its Roche lobe	[29]
4.3 ± 0.7	Light curve	[29]
2.68 ± 0.16	Parallax	[43]

of sight (see the discussion in [40]). This is however at odds with the expansion velocity of the synchrotron shock, as it was pointed out by [42], in which they derived a distance of (2.45 ± 0.37) kpc. Given all these caveats, in the subsequent calculations we assume the distance to be 2.45 kpc.

B Observations and data analysis

In this section we report the detailed results of the analysis of gamma-ray data with MAGIC and *Fermi*-LAT, and optical data with TJO and ANS.

B.1 MAGIC

MAGIC [44] is a stereoscopic system of two imaging atmospheric Cherenkov telescopes situated in the Canary island of La Palma, Spain (28.8°N, 17.9°W at 2225 m above sea level). Each telescope consists of a 17-m diameter mirror dish and a fast imaging camera. The system achieves a sensitivity of $(0.92 \pm 0.04)\%$ of the Crab Nebula flux above 210 GeV in 50 h in zenith angle range $30 - 45°$ [45].

MAGIC observed RS Oph in the period between August 09, 2021 to September 01, 2021 (MJD 59435.93 to 59458.97) for 34.0 h (see Table 2). The data quality selection was based on the atmospheric transmission and rates of background events. For this analysis we also did not include data taken under moonlight condition, as they provide much higher energy threshold values. After quality cuts, 21.4 h of the data were used for the analysis, half of which were taken during the first four days after the nova eruption. The source was observed at zenith angles between 36° and 60°. The data were taken in the so-called wobble mode, pointing at four different sky positions situated 0.4° away from the source to evaluate the background simultaneously.

The data were analyzed using the MAGIC Analysis and Reconstruction Software, MARS [46]. A dedicated low-energy procedure with a special signal extraction and image cleaning, the so-called MaTaJu method, was applied (see [47] and references therein). Further processing of the data, including the image parameterization, the direction and energy reconstruction and gamma-hadron separation, were applied following the standard MARS analysis chain. The energy threshold of the analysis is ∼60 GeV.

RS Oph is detected with a significance of $13.2\,\sigma$ (see Fig. 4). We fitted the

Table 2 Summary of the MAGIC observation campaign: time of observation slot, observation conditions, total observation time during the slot, effective time after the data selection (only Dark data).

MJD Start - End	Obs. conditions	Obs. time [h]	Time after cuts [h]
59435.94 - 59435.98	Dark	1.0	1.0
59436.89 - 59437.04	Dark	3.6	3.5
59437.89 - 59438.03	Dark	3.2	3.1
59438.88 - 59439.02	Dark	3.2	3.2
59439.89 - 59440.02	Dark + Moon	3.0	-
59440.89 - 59441.02	Dark + Moon	3.0	-
59444.89 - 59444.91	Moon	0.1	-
59445.88 - 59445.90	Moon	0.2	-
59451.89 - 59452.00	Dark + Moon	2.1	0.5
59452.88 - 59453.01	Dark + Moon	2.9	1.6
59453.88 - 59454.00	Dark + Moon	2.7	2.0
59454.87 - 59454.98	Dark	2.5	-
59455.87 - 59455.97	Dark	2.3	2.3
59456.87 - 59456.97	Dark	2.3	2.3
59458.89 - 59458.97	Dark	1.9	1.9

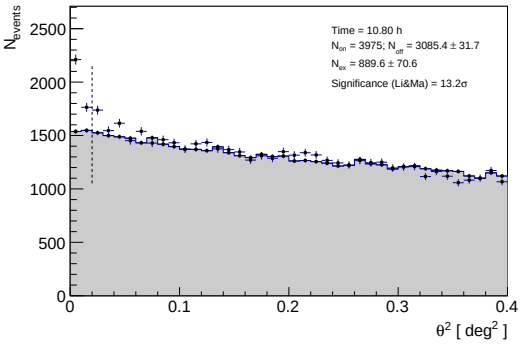

Fig. 4 Distribution of the squared angular distance between the nominal source position and the reconstructed arrival direction of events (black crosses) and the estimated background (gray shaded area). Vertical dashed line represents the angular cut below which the number of background and excess events as well as the statistical significance of the detection are given (inset panel).

spectrum obtained from the first four days of observations using a single power-law ($\mathrm{d}N/\mathrm{d}E = f_0\ (E/E_0)^{-\alpha}$), resulting with a $\chi^2/\mathrm{N_{dof}} = 5.9/5$ goodness of fit[1]. The normalization energy of the fit ($E_0 = 130\,\mathrm{GeV}$) is the decorrelation energy (i.e. normalization energy which minimizes the correlation of the fit parameters) of the four-day sample. The fit parameters are listed in Table 3.

We have also performed night-by-night spectral fits to investigate spectral variability. The parameters from the first two nights are consistent within errors (note however that the exposure on the first night is lower than on the remaining ones). A hint of hardening of the emission is seen between the second

[1]The used fit also takes into account estimated energy bins without detected signal, hence the number of degrees of freedom is larger than expected from the number of points in the reconstructed spectrum.

Table 3 Spectral fit results (normalization f_0 at $E_0 = 130\,\mathrm{GeV}$, and photon index α) of MAGIC data: daily and the combined emission from the first four days.

MJD	f_0 [10^{-10} TeV^{-1}cm^{-2}s^{-1}]	α	$\chi^2/\mathrm{N_{dof}}$
59435.94 - 59435.98	$5.0^{+1.3}_{-1.5}$	$3.92^{+0.51}_{-0.68}$	5.6/5
59436.89 - 59437.04	$3.73^{+0.92}_{-0.94}$	$4.71^{+0.34}_{-0.42}$	5.1/5
59437.89 - 59438.03	$5.03^{+0.81}_{-0.80}$	$3.70^{+0.28}_{-0.32}$	3.6/5
59438.88 - 59439.02	$4.83^{+0.77}_{-0.77}$	$3.78^{+0.25}_{-0.28}$	10.3/5
59435.94 - 59439.02	$4.66^{+0.47}_{-0.48}$	$4.07^{+0.18}_{-0.20}$	5.9/5

and third night. No significant change of parameters can be seen between the third and the fourth night.

The daily-binned light curve was calculated for an integral flux above 100 GeV. For the first four days the fit to a constant flux gives a $\chi^2/\mathrm{N_{dof}} = 2.9/3$ with a value of $F_0 = (4.41 \pm 0.46_{\mathrm{stat}}) \times 10^{-11}\,\mathrm{cm^{-2}\,s^{-1}}$.

B.2 *Fermi*-LAT

The Large Area Telescope on-board the *Fermi* Gamma-ray Space Telescope (*Fermi*-LAT), is a pair conversion telescope designed to detect gamma rays with an energy range of 0.02 GeV to $>$ 300 GeV [48]. The *Fermi*-LAT, with its large field of view (2.4 sr), observes the entire sky approximately every 3 hours [2]. Each analysis is performed with *fermitools* v2.0.8[3] and *Fermipy* v1.0.2 [49] using a binned likelihood analysis, P8R3_V3 instrument response functions (IRFs), and the catalog 4FGL-DR2 [50, 51] with the standard Galactic and isotropic diffuse background to construct the model of the region of interest (ROI).

For the 1-day and 3-day time bins, the *Fermi*-LAT data-set used encompasses a total time range from MJD 59431.45 to 59461.45, an energy range from 0.1 GeV to 1000 GeV, and a 15° ROI centered on the radio coordinates of RS Oph (R.A. = 267.555°, Dec. = -6.7078°). The *SOURCE* event class and event type 3 are used for this analysis and we select a maximum zenith angle of $>$ 90° to reduce any gamma-ray contamination from the Earth limb. The majority of 4FGL-DR2 sources for the one and three day time bins are not significantly detected (Test Statistic (TS)[4] $>$ 25, see [52]), apart from 4FGL J1813.4-1246 and 4FGL J1745.4-0753. These sources correspond to PSR J1813-1246 and TXS 1742-078, which are 8.3° and 1.7° away from RS Oph. TXS 1742-078 is a non-variable hard blazar and therefore could cause possible source confusion. Due to the proximity of 4FGL J1745.4-0753 to RS Oph and possible source confusion at the lowest energies, the value of the index of 4FGL J1745.4-0753 is locked to that of the 4FGL-DR2 catalog. RS Oph is included in the ROI and modeled with a Log Parabola model. Additional spectral models were tested for four-day period contemporaneous to MAGIC

[2] https://fermi.gsfc.nasa.gov/ssc/observations/types/post_anomaly/

[3] https://fermi.gsfc.nasa.gov/ssc/data/analysis/software/

[4] TS = -2 ln ($\mathcal{L}_{max,0}/\mathcal{L}_{max,1}$), where $\mathcal{L}_{max,0}$ is the maximum likelihood of the null hypothesis and $\mathcal{L}_{max,1}$ is the maximum likelihood with the source included [52]. The square-root of the TS is approximately equal the significance of detection, i.e. a TS = 25 is $\sim 5\,\sigma$.

observations: a power-law (TS= 2168.1) as well as a power-law with an exponential cutoff (TS= 2016.4), and the Log Parabola model (TS= 2226.44) had the highest TS. The ROI is optimized with the normalization and spectral parameters of any 4FGL-DR2 source with a number of predicted counts $<$ 1 locked to the 4FGL-DR2 values, excluding the Galactic and isotropic diffuse background. All parameters on all unlocked 4FGL-DR2 sources within 4° are left free to vary, and the ROI is fit using *Minuit* minimizer. If RS Oph source model does not have a TS $>$ 9, number of predicted counts $>$ 4 or the error of the integrated flux from 0.1 GeV to 1000 GeV is greater than 60% of the value, then it is not considered detected and 95% upper limits (ULs) are calculated. These 1-day and 3-day light curves are presented in Tables 4 and 5 and in Fig. 1. The 1-day light curve in MJD 59435.45–59444.45 range can be well fit ($\chi^2/\mathrm{N_{dof}} = 6.5/7$) with an exponential decay with halving time of (2.20 ± 0.18) days. The associated SEDs for the first four days are presented in Fig. 13.

The analysis of the combined first four days has a data-set which encompasses a time range MJD 59435.45 – 59439.45 and an energy range from 0.05 GeV to 1000 GeV. The same procedure is applied as in the 1-day and 3-day time bins, with some adjustments in the settings to allow the analysis to reach 0.05 GeV. Due to the worsening of the *Fermi*-LAT PSF below 0.1 GeV, we apply a 20° ROI centered on RS Oph, and a more restrictive zenith angle selection of $>$ 80°. We perform a joint-likelihood analysis with two components, one in the energy range between 0.05 GeV to 0.1 GeV and one in the energy range from 0.1 GeV to 1000 GeV. We remove *PSF0* and *PSF1* event types from the analysis below 0.1 GeV and keep all event types above 0.1 GeV. This reduces the possibility of source confusion from nearby weak sources. The obtained SEDs are presented in Fig. 3.

B.3 Optical photometry

Optical photometric observations of RS Oph were carried out by Joan Oró Telescope (TJO) and *Asiago Novae & Symbiotic stars Collaboration* (ANS, telescopes ID 310, 610 and 2203). The TJO is a 1-meter class robotic telescope located at Montsec observatory (42.05°N, 0.73°E), Catalonia, Spain. The multi band (*BVRI*) data were analysed using a semi-automatic pipeline for differential photometry [53] assuming the aperture radius of 7.5″, the comparison stars marked in Fig. 5, and the comparison star magnitudes listed in Table 6. The observed magnitude of the source is reported in Table 7 and the *V*-band light-curve is illustrated in Fig. 1 (bottom panel), as an example, together with the data obtained from American Association of Variable Star Observers International Database (AAVSO).

The data obtained by ANS are analyzed using PSF photometry method described in [54, 55]. The same local photometric sequence, extracted from APASS DR8 all-sky survey [56, 57] and accurately placed on the system of equatorial standards [58] via the color equations calibrated in [59, 60], has

Table 4 *Fermi*-LAT 1-Day Average Integral Flux. Values with * are fixed in the UL calculation.

MJD Start - End	TS	Integral Flux (> 0.1 GeV) (10^{-7} photons cm^{-2} s^{-1})	α	β
59431.45 - 59432.45	0.4	< 11.0	2.0*	0.0*
59432.45 - 59433.45	0.0	< 10.8	2.0*	0.0*
59433.45 - 59434.45	0.0	< 10.7	2.0*	0.0*
59434.45 - 59435.45	191.2	18.8 ± 3.1	2.16 ± 0.13	0.054 ± 0.076
59435.45 - 59436.45	1006.9	46.4 ± 3.9	1.96 ± 0.078	0.197 ± 0.051
59436.45 - 59437.45	501.0	39.3 ± 4.3	2.123 ± 0.099	0.175 ± 0.066
59437.45 - 59438.45	433.4	27.4 ± 3.4	1.955 ± 0.095	0.169 ± 0.065
59438.45 - 59439.45	197.8	17.9 ± 3.4	2.12 ± 0.16	0.24 ± 0.12
59439.45 - 59440.45	172.3	12.8 ± 2.7	1.96 ± 0.16	0.22 ± 0.11
59440.45 - 59441.45	94.6	7.3 ± 2.3	1.63 ± 0.21	0.16 ± 0.11
59441.45 - 59442.45	97.6	12.2 ± 3.2	1.99 ± 0.17	0.15 ± 0.12
59442.45 - 59443.45	60.3	4.3 ± 1.6	1.96 ± 0.42	0.95 ± 0.58
59443.45 - 59444.45	82.0	5.5 ± 1.9	1.58 ± 0.28	0.39 ± 0.21
59444.45 - 59445.45	2.5	< 11.4	2.0*	0.0*
59445.45 - 59446.45	24.9	10.0 ± 4.1	2.65 ± 0.61	0.18 ± 0.33
59446.45 - 59447.45	16.0	< 11.9	2.0*	0.0*
59447.45 - 59448.45	17.1	< 11.7	2.0*	0.0*
59448.45 - 59449.45	28.5	< 12.1	2.0*	0.0*
59449.45 - 59450.45	3.2	< 11.5	2.0*	0.0*
59450.45 - 59451.45	27.6	4.0 ± 2.3	1.93 ± 0.34	0.16 ± 0.22
59451.45 - 59452.45	0.7	< 11.2	2.0*	0.0*
59452.45 - 59453.45	2.4	< 11.1	2.0*	0.0*
59453.45 - 59454.45	13.3	< 11.3	2.0*	0.0*
59454.45 - 59455.45	20.2	6.1 ± 3.1	2.48 ± 0.49	0.15 ± 0.28
59455.45 - 59456.45	5.0	< 11.6	2.0*	0.0*
59456.45 - 59457.45	7.5	< 11.7	2.0*	0.0*
59457.45 - 59458.45	1.0	< 11.0	2.0*	0.0*
59458.45 - 59459.45	5.8	< 11.7	2.0*	0.0*
59459.45 - 59460.45	6.1	< 11.6	2.0*	0.0*
59460.45 - 59461.45	12.8	4.2 ± 2.3	2.26 ± 0.46	0.51 ± 0.26
59461.45 - 59462.45	8.3	< 11.3	2.0*	0.0*
59462.45 - 59463.45	4.4	< 11.4	2.0*	0.0*
59463.45 - 59464.45	4.6	< 11.5	2.0*	0.0*
59464.45 - 59465.45	1.9	< 10.8	2.0*	0.0*

Table 5 *Fermi*-LAT 3-Day Average Integral Flux. Values with * are fixed in the UL calculation.

MJD Start - End	TS	Integral Flux (> 0.1 GeV) (10^{-7} photons cm^{-2} s^{-1})	α	β
59431.45 - 59434.45	0.0	< 10.5	2.0*	0.0*
59434.45 - 59437.45	1621.7	34.0 ± 2.1	2.041 ± 0.053	0.160± 0.040
59437.45 - 59440.45	797.5	19.7 ± 1.8	1.999 ± 0.072	0.200± 0.051
59440.45 - 59443.45	244.0	8.2 ± 1.5	1.83 ± 0.12	0.200± 0.084
59443.45 - 59446.45	80.6	4.0 ± 1.3	1.90 ± 0.22	0.28± 0.16
59446.45 - 59449.45	49.0	1.62 ± 0.67	1.47 ± 0.40	0.55± 0.32
59449.45 - 59452.45	25.4	2.3 ± 1.3	2.01 ± 0.32	0.16± 0.20
59452.45 - 59455.45	27.4	2.0 ± 1.2	1.93 ± 0.29	0.03± 0.13
59455.45 - 59458.45	11.3	< 10.8	2.0*	0.0*
59458.45 - 59461.45	10.8	< 11.6	2.0*	0.0*
59461.45 - 59464.45	9.0	< 11.2	2.0*	0.0*

Table 6 Comparison stars magnitudes used in differential photometry procedure for TJO data. Values are obtained from AAVSO.

Star	B	V	R	I
115	12.242 ± 0.012	11.517 ± 0.008	11.078± 0.011	10.660 ± 0.014
121	12.967 ± 0.011	12.126 ± 0.009	11.590 ± 0.017	11.029 ± 0.020
129	13.755 ± 0.015	12.900 ± 0.014	12.342 ± 0.015	11.750 ± 0.021
130	13.924 ± 0.013	13.011 ± 0.011	12.430 ± 0.018	11.844 ± 0.021
133	14.273 ± 0.012	13.254 ± 0.008	12.586 ± 0.011	11.934 ± 0.013

been used for all telescopes ensuing a high consistency of the data. The photometry results are given in Table 7, where the quoted uncertainties are the total error, which quadratically combine the measurement error on the variable with the error associated to the transformation from the instantaneous local photometric system to the standard one (as defined by the photometric comparison sequence). All measurements were carried out with aperture photometry. The resulting light- and color-curves are plotted in Fig. 6, where they are compared to the similar data for the 2006 event as published in [61].

The cross calibration between instruments was performed by using the color index of the source. The data obtained by two telescopes are in good agreement. However, to reduce the systematic uncertainties, minimal offsets ($B - V = +0.03$, $V - R = +0.05$, and $V - I = -0.02$) were applied to TJO data. The contribution of the strongest emission lines (H_α and H_β) were removed from the observed magnitude using the simultaneous spectroscopic observations from the publicly available optical spectra in Astronomical Ring for Access to Spectroscopy (ARAS) [62]. We found that the contribution of the H_β emission line in the V-band is negligible for the first ten days after the outburst. The contribution of the H_β emission line is significant in the B-band and increases from 3% to 15% during the same time interval. Moreover, the contribution of the H_α emission line is dominant in the R-band and increases from 5% to 83% during the same time interval owing to a sudden jump from 5% to 34% between $T - T_0 = 0.98$ days and $T - T_0 = 2.89$ days. The results of these corrections are presented in Table 8.

All optical data described in this section are corrected for the effect of Galactic extinction by assuming $E(B-V) = 0.65$ [63], Galactic extinction law [64], and the absolute fluxes (corresponding to zero magnitude) [65] in each band.

During the nova outburst the photosphere emission creates the dominant radiation field. We describe the radiation field using photometric and spectroscopic measurements by applying black body approximation. During the first four days of the nova, contemporaneous with the MAGIC measurements, the emission can be described by the photosphere temperature dropping from $T_{ph} = 10800$ K to 7680 K and radius $R_{ph} = 200\, R_\odot$ (see Fig. 7). The photosphere fit of 2006 eruption [66], when rescaled to the nova distance of 2.45 kpc, provides a similar radius $(245 - 310)\, R_\odot$, and temperature (8200 K).

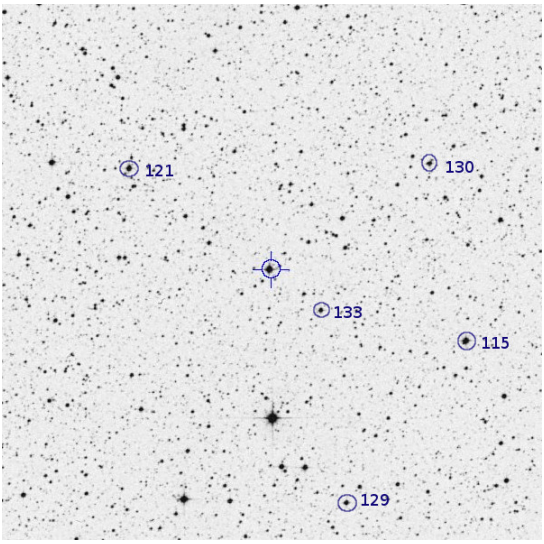

Fig. 5 Optical finding chart of RS Oph used for differential photometry.

B.4 Spectroscopy and spectropolarimetry

RS Oph spectra during the 2021 outburst have been acquired with the Echelle spectrograph of the Varese 0.84 m telescope [67], the Catania Astrophysical Observatory Spectropolarimeter [68] of the Catania 0.91 m telescope and HARPS-North [69] of the Telescopio Nazionale Galileo. The reduction of spectra, which included the subtraction of the bias frame, trimming, correcting for the flat-field and the scattered light, extraction for the orders, and wavelength calibration, was done as in [70] by using the NOAO/IRAF packages[5]. The log-book of observations is in Table 9.

B.4.1 Kinematics

The H_α profile obtained on day $T - T_0 = 0.91$ consists of a triangular shape with Full Width at Zero Intensity of $\sim 7500\,\mathrm{km\,s^{-1}}$ and a blue shift absorption component at $4250\,\mathrm{km\,s^{-1}}$, exactly as it was reported by [71] 1.38 days after the 2006 outburst of RS Oph. The close similarity of the 2006 and 2021 spectral line profiles along the envelope expansion is testified on day $T - T + 0 = 15$ by the presence of satellite components at the same high-velocity ($2500\,\mathrm{km\,s^{-1}}$). This feature was associated by [71] to a presence of two jets (c.f. figs. 1 and 2 therein and Fig. 8). Also, [72] measured a velocity of $4200\,\mathrm{km\,s^{-1}}$ the day after the outburst.

Because of the day-by-day changing of absorption and emission features across the whole RS Oph spectrum, we have determined the velocity of the expanding envelope as the terminal value simultaneously representative of the

[5]IRAF is distributed by the National Optical Astronomy Observatory, which is operated by the Association of Universities for Research in Astronomy, Inc.

Table 7 The observed optical magnitude of RS Oph.

MJD	Telescope	B	V	R	I
59435.913	ANS	5.667 ± 0.011	4.884 ± 0.014	4.194 ± 0.016	3.544 ± 0.018
59437.824	ANS	6.611 ± 0.011	5.855 ± 0.014	4.816 ± 0.016	4.164 ± 0.020
59437.850	ANS	6.508 ± 0.013	5.811 ± 0.022	4.801 ± 0.028	4.167 ± 0.032
59438.820	ANS	6.968 ± 0.034	6.321 ± 0.045	4.966 ± 0.046	4.611 ± 0.054
59438.845	ANS	6.871 ± 0.012	6.215 ± 0.024	4.982 ± 0.036	4.459 ± 0.030
59439.812	ANS	7.288 ± 0.014	6.637 ± 0.017	5.270 ± 0.019	4.856 ± 0.020
59439.881	TJO	7.303 ± 0.012	6.605 ± 0.011	-	4.850 ± 0.015
59440.817	TJO	-	6.895 ± 0.015	5.482 ± 0.014	5.103 ± 0.011
59440.818	ANS	7.555 ± 0.008	6.923 ± 0.009	5.421 ± 0.011	5.050 ± 0.014
59440.840	ANS	7.445 ± 0.008	6.808 ± 0.014	5.285 ± 0.026	4.911 ± 0.021
59441.817	TJO	-	7.137 ± 0.020	5.587 ± 0.014	5.291 ± 0.013
59442.886	TJO	-	7.328 ± 0.011	-	-
59442.936	TJO	7.974 ± 0.012	7.335 ± 0.011	5.704 ± 0.011	5.431 ± 0.011
59443.824	ANS	8.053 ± 0.008	7.436 ± 0.010	5.745 ± 0.011	5.537 ± 0.014
59443.886	TJO	8.014 ± 0.012	7.359 ± 0.011	5.740 ± 0.011	5.537 ± 0.011
59444.313	ANS	8.129 ± 0.008	7.508 ± 0.009	5.797 ± 0.011	5.618 ± 0.014
59444.926	TJO	8.184 ± 0.013	7.616 ± 0.011	5.881 ± 0.011	5.719 ± 0.011
59445.849	TJO	-	7.688 ± 0.012	5.967 ± 0.011	5.782 ± 0.011
59446.826	ANS	8.367 ± 0.010	7.752 ± 0.012	6.003 ± 0.014	5.875 ± 0.016
59446.897	TJO	8.381 ± 0.013	7.695 ± 0.011	6.011 ± 0.011	5.867 ± 0.011
59447.807	ANS	8.582 ± 0.008	7.893 ± 0.010	6.115 ± 0.012	6.037 ± 0.014
59447.917	TJO	8.557 ± 0.014	7.914 ± 0.012	6.105 ± 0.011	6.024 ± 0.011
59449.808	ANS	8.655 ± 0.008	7.961 ± 0.014	6.157 ± 0.016	6.139 ± 0.014
59449.899	TJO	8.719 ± 0.028	8.193 ± 0.019	6.255 ± 0.013	-
59452.824	ANS	8.993 ± 0.007	8.431 ± 0.009	6.374 ± 0.014	6.492 ± 0.015
59454.882	TJO	9.027 ± 0.012	8.433 ± 0.011	-	-
59456.813	ANS	9.106 ± 0.008	8.532 ± 0.016	6.645 ± 0.017	6.728 ± 0.018
59458.804	ANS	9.181 ± 0.016	8.594 ± 0.019	6.535 ± 0.048	6.774 ± 0.038
59459.801	ANS	9.277 ± 0.009	8.748 ± 0.010	6.792 ± 0.011	6.984 ± 0.012
59459.805	ANS	9.305 ± 0.016	8.695 ± 0.018	6.641 ± 0.051	6.899 ± 0.041
59459.834	ANS	9.385 ± 0.007	8.879 ± 0.008	6.862 ± 0.009	7.043 ± 0.014
59460.801	ANS	9.403 ± 0.009	8.848 ± 0.015	6.894 ± 0.016	7.086 ± 0.017
59460.808	ANS	9.461 ± 0.007	8.958 ± 0.008	6.913 ± 0.010	7.148 ± 0.014
59460.871	TJO	9.361 ± 0.013	8.918 ± 0.011	6.972 ± 0.011	7.134 ± 0.011
59461.825	ANS	9.597 ± 0.007	8.997 ± 0.014	7.039 ± 0.015	7.230 ± 0.016
59462.796	ANS	9.690 ± 0.033	9.070 ± 0.043	6.995 ± 0.070	7.228 ± 0.054
59463.805	ANS	9.627 ± 0.008	9.087 ± 0.011	7.095 ± 0.012	7.307 ± 0.012
59463.883	ANS	9.789 ± 0.010	9.296 ± 0.018	7.299 ± 0.021	7.459 ± 0.024
59465.791	ANS	9.781 ± 0.017	9.161 ± 0.021	7.089 ± 0.034	7.363 ± 0.039

H_α, H_β and He I 5876λ P-Cygni profiles (Table 9). An error of 250 $km\,s^{-1}$ was assumed as representative of differences between profiles. Results are in Table 9. Fig. 8 shows these profiles in the first three days after the expansion as well as on days 5 and 15. The terminal velocity in time is given in the bottom right panel of Fig. 8.

The acceleration along the initial three days is not statistically confirmed and we assume $(4500 \pm 250)\,km\,s^{-1}$ as representative of the ejecta expansion at the earliest stage (during the VHE gamma-ray detection by MAGIC).

It is worth to remind that this velocity is volume average, weighted by the brightness, temperature and density of the ejecta velocities and agrees with results from the modeling by [73] of the HST images of the spatially resolved

Table 8 The observed optical magnitude (B and R band) of RS Oph after removing the contribution of H_α and H_β emission lines.

MJD	Telescope	H_β/B (%)	B	H_α/R (%)	R
59435.913	ANS	3	5.698 ± 0.011	5	4.247 ± 0.016
59437.824	ANS	9	6.701 ± 0.011	31	5.134 ± 0.016
59437.850	ANS	9	6.598 ± 0.013	34	5.093 ± 0.028
59438.820	ANS	11	7.081 ± 0.034	48	5.393 ± 0.046
59438.845	ANS	11	6.984 ± 0.012	48	5.409 ± 0.036
59439.812	ANS	11	7.405 ± 0.014	48	5.694 ± 0.019
59439.881	TJO	11	7.420 ± 0.012	-	-
59440.817	TJO	-	-	69	6.054 ± 0.014
59440.818	ANS	12	7.676 ± 0.008	69	5.993 ± 0.011
59440.840	ANS	12	7.566 ± 0.008	69	5.857 ± 0.026
59441.817	TJO	-	-	87	6.268 ± 0.014
59442.936	TJO	13	8.103 ± 0.012	91	6.407 ± 0.011
59443.824	ANS	14	8.192 ± 0.008	89	6.434 ± 0.011
59443.886	TJO	14	8.153 ± 0.012	89	6.429 ± 0.011
59444.313	ANS	14	8.268 ± 0.008	89	6.486 ± 0.011
59444.926	TJO	14	8.330 ± 0.013	83	6.538 ± 0.011

Table 9 Log-book of spectroscopic observations, and terminal velocity of the H_α, H_β and He I 5876λ P-Cygni profiles. A conservative error of 250 km s^{-1} has been associated to all velocities.

Telescope	TNG	Serra la Nave	Varese	
Spectrograph	HARPS-N	CAOS	Echelle	
R $= \lambda/\Delta\lambda$	115 000	45 000	18 000	
Range	370-690 nm	400-900 nm	425-890 nm	
	MJD			Terminal velocity [km s^{-1}]
			59435.837	4250
			59436.820	4600
			59437.807	4750
			59438.830	4000
			59439.808	3000
	59440.907		59440.867	2800
			59441.810	2700
		59442.838	59442.824	2700
		59443.821	59443.806	2700
		59444.850	59444.810	2600
		59445.852	59445.853	2500
		59446.817	59446.808	2500
			59447.801	2500
			59448.796	2400
			59449.794	2400
		59450.822	59450.814	2400
			59451.796	2400
			59452.785	2400
		59454.804		2300
		59455.792		2300
		59459.858		2100
		59467.830		2100
		59470.835		2000

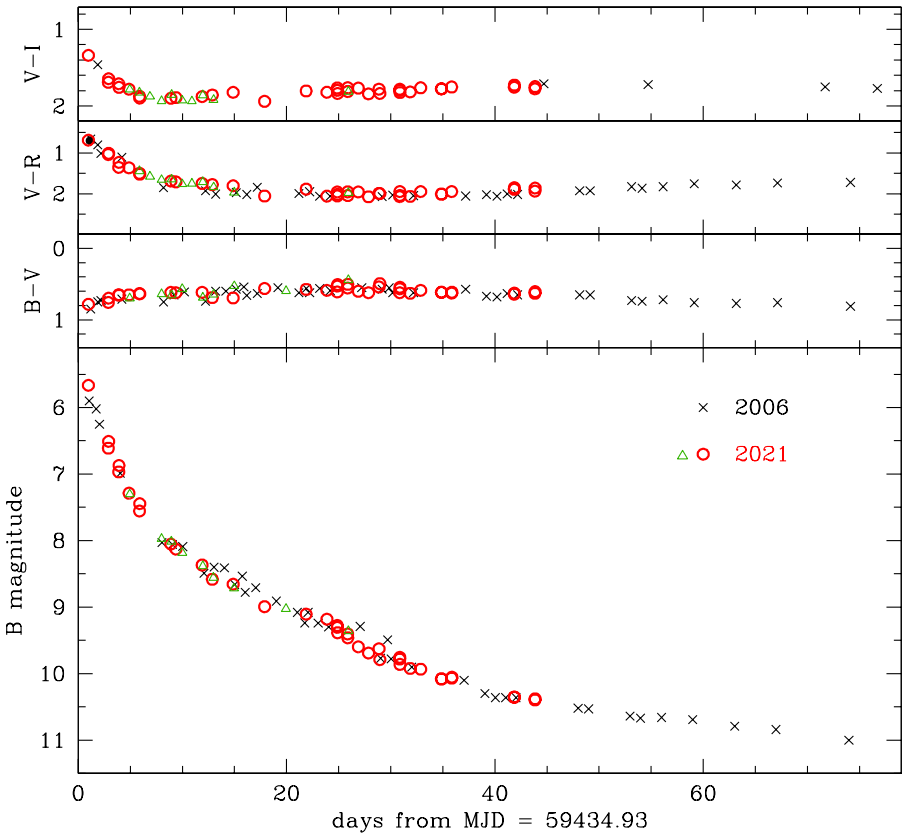

Fig. 6 Optical *B*-band observed magnitude and the color index of RS Oph 2021 outburst from ANS (red circles) and TJO (green triangle) compared to that of 2006 eruption (black crosses, computed with respect to MJD of 53775.86, [61]).

and expanding ejecta during the 2006 event. Radio maps of the 2006 outburst of RS Oph [74] have shown the presence of highly collimated flows with a velocity close to 10000 km s^{-1}. In this framework, the decrement of the velocity after the initial days with a linear trend, $V = 2990 - 27.6(T - T_0)$[km s^{-1}], is simply a consequence of a non-spherical mass outflow [71, 73, 75].

B.4.2 Temperature

We observe a large series of spectral lines in emission. The low ionization species peak in strength at the beginning of the expansion and are related to the wind of the RG. In the latest data, the spectral lines of highly ionized spectra carried out from the inner regions peaks in intensity. We find evidence of the forbidden spectral lines: [Fe XIV] at 5303 Å and [Ar X] at 5535 Å indicative of a temperature larger than 4MK (the ionization energy of Fe XIII and Ar IX are 361.0 eV and 422.6 eV, respectively).

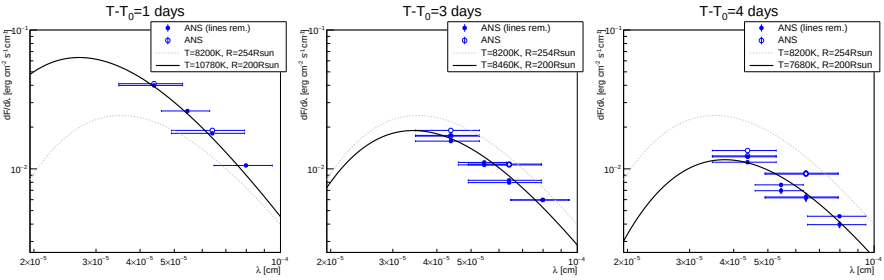

Fig. 7 Optical photometry performed by ANS 1, 2, and 4 days after the outburst (blue empty markers) corrected for the Galactic absorption. Filled markers show the flux after subtraction of Hα and Hβ line contributions. The thick black lines show a black-body emission used in the modeling, while the dashed line shows for comparison the average 2006 spectral fit from [66] (with the photosphere radius corrected to the distance of 2.45 kpc).

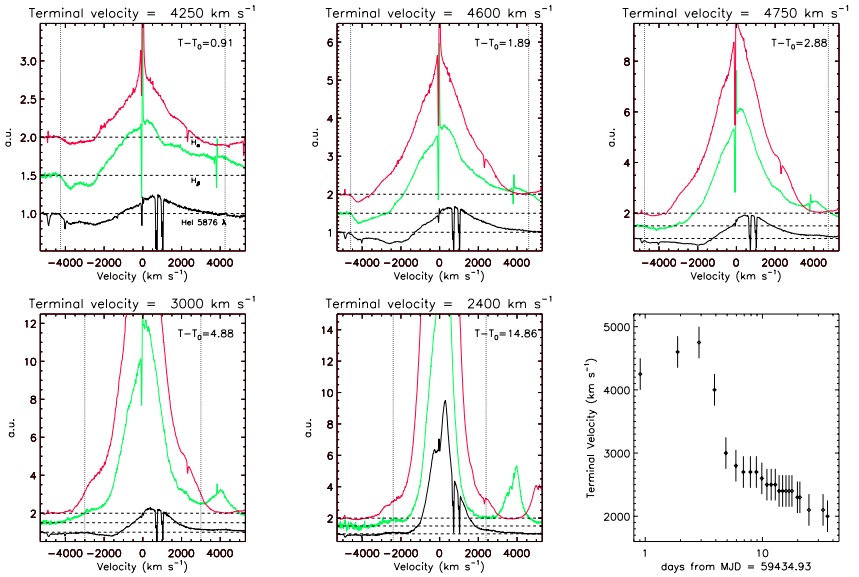

Fig. 8 Example of H$_\alpha$, H$_\beta$ and He I 5876λ P-Cygni profiles used to determine the behavior of the terminal velocity of the expanding envelope. The bottom right panel shows the evolution of the velocity in time.

B.4.3 The magnetic field

We have carried out high-resolution linear spectropolarimetry of RS Oph on MJD 59441.5 and 59442.5. Because of the presence of spectral lines in emission, we have adopted the observation and reduction procedures described in [76]. No polarization has been detected across any spectral lines. If we assume that linear polarization is due to a magnetic field and we apply the method described in [77], an upper limit of 750 G can be defined for the average of the transverse component of the field.

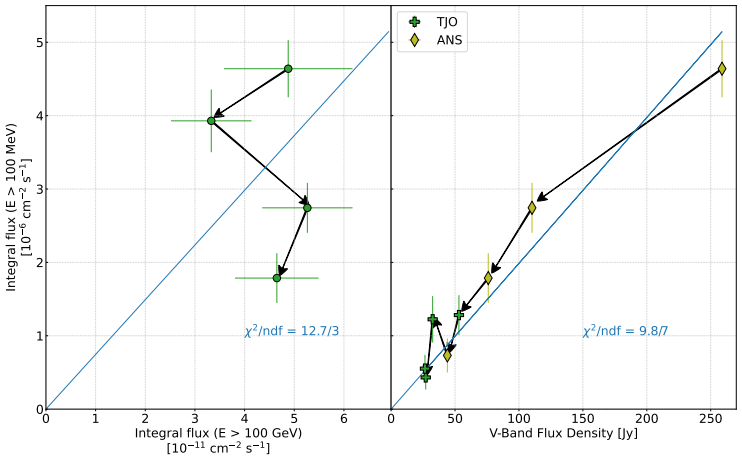

Fig. 9 Left panel: Comparison of the photon flux measured by MAGIC above 100 GeV with the one measured by *Fermi*-LAT above 100 MeV for the first four days of the outburst. Right panel: Comparison of the flux measured by *Fermi*-LAT $>$ 100 MeV with that of the V-band obtained by ANS. Arrows show the sequence of the flux temporal evolution and the blue line shows the linear proportionality fit in both panels.

Table 10 Daily *Fermi*-LAT and MAGIC joint spectral fit results. Individual columns give normalization f_0 at normalization energy $E_0 = 130$ GeV, slope α at E_0, curvature parameter β and goodness of fit ($\chi^2/\mathrm{N_{dof}}$).

MJD	$f_0[10^{-10}\mathrm{TeV^{-1}cm^{-2}s^{-1}}]$	α	β	$\chi^2/\mathrm{N_{dof}}$
59435.94 - 59435.98	5.4 ± 1.3	3.86 ± 0.13	0.194 ± 0.019	6.1/6
59436.89 - 59437.04	4.54 ± 0.78	3.73 ± 0.11	0.175 ± 0.020	16.4/6
59437.89 - 59438.03	5.37 ± 0.85	3.64 ± 0.12	0.173 ± 0.020	3.7/6
59438.88 - 59439.02	5.00 ± 0.78	3.44 ± 0.14	0.147 ± 0.027	10.8/6
59435.94 - 59439.02	5.08 ± 0.45	3.697 ± 0.059	0.175 ± 0.010	9.3/6

B.5 Multiwavelength view

In Fig. 9, we compare the integral fluxes (obtained from daily spectral fits) of *Fermi*-LAT and MAGIC. Fitting the relation with a linear proportionality ($F(> 100\,\mathrm{GeV}) \propto F(> 0.1\,\mathrm{GeV})$) we obtain $\chi^2/\mathrm{N_{dof}} = 12.7/3$. Therefore simple, achromatic gamma-ray variability is unlikely (chance probability $p = 5.3 \times 10^{-3}$).

We also perform a joint fit of *Fermi*-LAT and MAGIC data with a Log Parabola function shape: $dN/dE = f_0 \times (E/E_0)^{-\alpha-\beta\ln(E/E_0)}$ with E_0 =130 GeV. The fits are summarized in Table 10.

In the right panel of Fig. 9, we compare the integral fluxes (obtained from daily spectral fits) of *Fermi*-LAT and the differential fluxes for the V-band obtained by ANS and TJO. We selected only the coincident data for MJD

59435 - 59445, for which the daily *Fermi*-LAT integral fluxes fulfill the condition not to calculate an upper limit. We fit a function $y = A\,x$ to the data that gives a $\chi^2/\mathrm{N_{dof}} = 9.8/7$.

Despite the data being consistent with a linear optical-GeV correlation, this does not provide a straight-forward interpretation about the underlying particle population producing this emission. As the ejecta propagate away from the WD, the radiation field seen at the shock will in fact decay faster than the observed at Earth optical emission. Moreover, as the electrons would cool faster (see Section C) than the observed decay of the radiation, we do not expect a linear relation between the IC emission and optical. The IC emission would rather follow the rate of injection of particles from the acceleration process. This correlation could therefore be related to ejecta or particle acceleration parameters.

C Modeling

Using the estimated parameters of the nova, we evaluate the conditions required to accelerate particles (electrons or protons) up to energies of hundreds of GeV using similar approach to [13, 20].

C.1 Acceleration and cooling of particles

We parametrize the acceleration of charged particles with acceleration parameter ξ:

$$\left(\frac{dE}{dt}\right)_{acc} = \frac{\xi c E}{R_L(E)}, \tag{1}$$

where $R_L(E)$ is the Larmor radius of particle with energy E in perpendicular magnetic field B. The corresponding acceleration time scale, expressed in days, can be computed as:

$$t_{acc} = E/\left(\frac{dE}{dt}\right)_{acc} = 3.9\left(\frac{E}{300\,\mathrm{GeV}}\right)\left(\frac{\xi B}{10^{-7}\,\mathrm{G}}\right)^{-1}\,[\mathrm{days}]. \tag{2}$$

The maximum achieved energies will stem from balancing such acceleration time with ballistic time t_{bal}, defined as the time from the onset of the nova, or by dominating cooling process. The shock distance R_{sh} at the time $t = T - T_0$ can be estimated based on its speed v_{sh}:

$$R_{sh} = 1.2\times10^{14}\left(\frac{v_{sh}}{4500\,\mathrm{km\,s^{-1}}}\right)\left(\frac{t}{3\,\mathrm{d}}\right)\,[\mathrm{cm}]. \tag{3}$$

As the nova shock expands the adiabatic energy losses will be directly connected with the ballistic time. We define the adiabatic time scale as the time in which the energy of particles decreases by a factor of e, resulting in $t_{adiab} = e\,t_{bal}$.

The protons will cool on hadronic interactions with the ambient matter, either the nova ejecta, or the RG wind. We assume that the ejecta concentrate at the distance of R_{sh} in a layer with a thickness of $h \times R_{sh}$, with $h = 0.1$. The number density of the ejecta can be estimated as:

$$n_{ej} = \frac{M_{ej}}{4\pi h R_{sh}^3 m_p} = 6.0\times10^8\,\frac{M_{ej}}{10^{-6}M_\odot}\left(\frac{v_{sh}}{4500\,\mathrm{km\,s^{-1}}}\right)^{-3}\left(\frac{t}{3\,\mathrm{d}}\right)^{-3}\left(\frac{h}{0.1}\right)^{-1}\,[\mathrm{cm^{-3}}], \tag{4}$$

where M_{ej} is the total ejected mass and m_p is the proton mass. Alternative assumption that the ejecta fill homogenously a sphere with radius R_{sh} would result in a factor of 3 lower value of n_{ej}. The number density of the ambient

material in the RG wind can be estimated as:

$$n_{RG} = \frac{\dot{M}_{RG}}{4\pi R_{sh}^2 v_{RG} m_p} = 0.22\times10^8 \frac{\dot{M}_{RG}}{10^{-7} M_\odot/\mathrm{yr}} \left(\frac{v_{sh}}{4500\,\mathrm{km\,s^{-1}}}\right)^{-2} \left(\frac{t}{3\,\mathrm{d}}\right)^{-2} \left(\frac{v_{RG}}{10\,\mathrm{km\,s^{-1}}}\right)^{-1} \quad (5)$$

where v_{RG} is the speed of the RG wind and $\dot{M}_{RG}$ is the mass loss rate of the RG. The total density of the ambient medium for the hadronic interaction is $n_p = n_{ej} + n_{RG}$, and for the expected parameters of RS Oph it is mostly dominated by the ejecta. The proton cooling time scale on hadronic p-p interactions can be then computed as:

$$t_{pp} = (n_p c \sigma_{pp})^{-1} = 21(n_p/6\times10^8\,\mathrm{cm^{-3}})^{-1}\,[\mathrm{days}], \quad (6)$$

where $\sigma_{pp} = 3\times10^{-26}\,\mathrm{cm^2}$. As the cooling timescale is longer than the ballistic time, the maximum energies to which protons can be accelerated are determined by the time from the nova onset.

In the case of electrons, cooling losses can originate either from inverse Compton scattering on the photosphere thermal radiation or from Bremsstrahlung radiation on the ambient matter. We compute the inverse Compton cooling time scale taking into account Klein-Nishina correction factor following [78]

$$t_{IC} = \frac{3(m_e c^2)^2}{4 c \sigma_T u_{ph} E} \left(1 + 4\epsilon_{ph} E/(m_e c^2)^2\right)^{1.5}, \quad (7)$$

where m_e is the electron mass. The total energy density, u_{ph}, and characteristic temperature of soft photons, ϵ_{ph}, can be estimated as

$$u_{ph} = 0.14 \frac{(R_{ph}/200\,R_\odot)^2 (T_{ph}/8460\,\mathrm{K})^4}{(v_{sh}/4500\,\mathrm{km\,s^{-1}})^2 (t/3\,\mathrm{d})^2} [\mathrm{erg\,cm^{-3}}] \quad (8)$$

$$\epsilon_{ph} = 2.2(T_{ph}/8460\,\mathrm{K})\,[\mathrm{eV}]. \quad (9)$$

For the used above scaling values the dependence of t_{IC} with energy can be described as $t_{IC} = 4.4\times10^{-3}(E/300\,\mathrm{GeV})^{-1})[1 + 10(E/300\,\mathrm{GeV})]^{1.5}$ [days] resulting in fast cooling of high-energy electrons. We estimate the Bremsstrahlung losses using the same density of ambient matter n_p as

$$t_{brems} = X_0/(n_p m_p c) = 24(n_p/6\times10^8\,\mathrm{cm^{-3}})^{-1}\,[\mathrm{days}], \quad (10)$$

where $X_0 = 63\,\mathrm{g\,cm^{-2}}$ is the radiation length in proton gas. For the expected parameters of RS Oph, the Bremsstrahlung losses are thus negligible. Also the synchrotron energy losses are negligible, unless the magnetic field in the shock reaches the level of a about 1 G.

The different time scales are summarized in Fig. 10. In order to accelerate protons up to energies of a few hundred GeV, the value of $\xi B \gtrsim 10^{-7}$ G

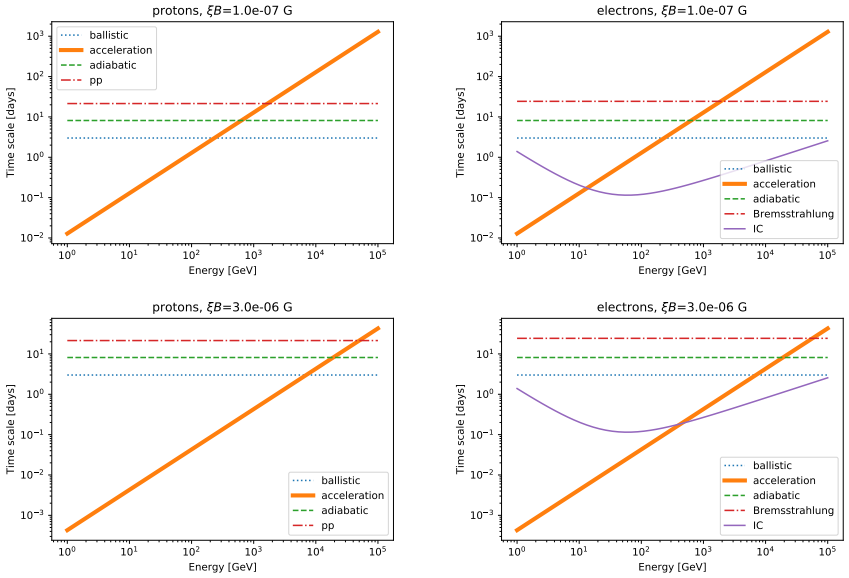

Fig. 10 Cooling and acceleration time scale for protons (left panels) and electrons (right panels) for two values of ξB parameter: 10^{-7} G (top panels) and 3×10^{-6} G (bottom panels). Assumed parameters (see text for details): $v_{sh} = 4500\,\mathrm{km\,s^{-1}}$, $t = 3\,\mathrm{d}$, $R_{ph} = 200\,R_\odot$, $T_{ph} = 8460\,\mathrm{K}$, $n_p = 6\times10^8\,\mathrm{cm^{-3}}$.

is required. If electrons are accelerated in the same conditions, they can reach energies of only ~ 10 GeV. In order to explain the observed gamma-ray emission reaching hundreds of GeV, much higher values $\xi B \gtrsim 3\times10^{-6}$ G are required. Second-order Fermi acceleration on the nova shock is expected to provide acceleration parameter of the order of $\xi \lesssim (v_{sh}/c)^2 \approx 10^{-4}$, resulting in the requirement of $B \gtrsim 0.03$ G fields for the electron case and much weaker $B \gtrsim$ mG for the proton one.

C.2 Energetics

The kinetic energy of the ejecta can be estimated as:

$$E_k = 0.5 M_{ej} v_{sh}^2 = 2.0\times10^{44}\left(\frac{M_{ej}}{10^{-6}M_\odot}\right)\left(\frac{v_{sh}}{4500\,\mathrm{km\,s^{-1}}}\right)^2 \mathrm{erg} \qquad (11)$$

For the assumed parameters determining the density of target material, the fit of the proton energy distribution in Fig. 3 requires a total power in protons of 4.4×10^{43} erg. This energetics requirement scales with the assumed model parameters as:

$$E_{p,nova} = 0.44\times10^{44}\left(\frac{M_{ej}}{10^{-6}M_\odot}\right)^{-1}\left(\frac{v_{sh}}{4500\,\mathrm{km\,s^{-1}}}\right)^{3}\left(\frac{d}{2.45\mathrm{kpc}}\right)^{-2}\frac{h}{0.1}\,\mathrm{erg} \qquad (12)$$

Therefore the efficiency of conversion of energy from the shock to protons can be computed as the ratio of the above two formulae:

$$\epsilon = \frac{E_{p,nova}}{E_k} = 0.22 \left(\frac{M_{ej}}{10^{-6} M_\odot}\right)^{-2} \left(\frac{v_{sh}}{4500\,\mathrm{km\,s^{-1}}}\right) \left(\frac{d}{2.45\mathrm{kpc}}\right)^{-2} \frac{h}{0.1} \quad (13)$$

It is clear that protons need to obtain a significant fraction ($\sim 20\%$) of the shock kinetic energy. Lower fraction could be achieved if the mass of the ejecta is higher, it is more concentrated at the shock (lower h) or if the speed of the shock is decreased.

C.2.1 Contribution to the Cosmic Ray sea

These accelerated protons eventually escape the nova to be part of the sea of Cosmic Rays. Since they do not suffer strong energy losses due to their interaction with intergalactic magnetic and photon fields, as it is the case for electrons, their contribution may extend to large distance from the nova explosion at all energies. Assuming that the energy released in all novae into accelerated protons is similar to that released in RS Oph ($E_{p,nova} = 4.4 \times 10^{43}$ erg) and we assume a nova rate of $\sim$100 per year [79] as an upper limit, we get a total of

$$\text{Novae energy rate} = E_{p,nova} \times \text{nova rate} = 4.4 \times 10^{45} [\text{erg/year}] \quad (14)$$

It is considered that a supernova explosion usually releases $E_{\rm SN} \sim 10^{51}$ erg [80], out of which $\sim$10% can be converted into accelerated protons at the shock between the supernova ejecta and the interstellar medium (ISM). The SN rate in the galaxy is $\sim$2 per century [81], therefore the supernova energy rate would be:

$$\text{Supernovae energy rate} = 0.1 \times E_{\rm SN} \times \text{supernova rate} = 2 \times 10^{48} [\text{erg/year}] \quad (15)$$

making the contribution of novae $\lesssim$0.2% to that of supernovae.

Let us now assume that the average energy density in CRs in the Milky Way is $E_{\rm dens,CRs} \sim 1$ eV/cm^3. We would like to compute what is the region in which the energy density of the protons accelerated by the nova dominates over this energy density. The energy density of these protons will be given by the total energy ($E_{p,nova}$) divided by the volume of the region

$$E_{\rm dens,nova,1\,eruption} = \frac{3 E_{p,nova}}{4\pi R^3_{\rm eruption}} \quad (16)$$

where $R_{\rm eruption}$ is the radius of the region. If we compare $E_{\rm dens,nova} = E_{\rm dens,CRs}$, we obtain $R_{\rm eruption} \sim$0.6 pc.

Finally, in the special case of a recurrent nova like RS Oph that repeats its explosions every 10 years, we would get this energy injection repeated over

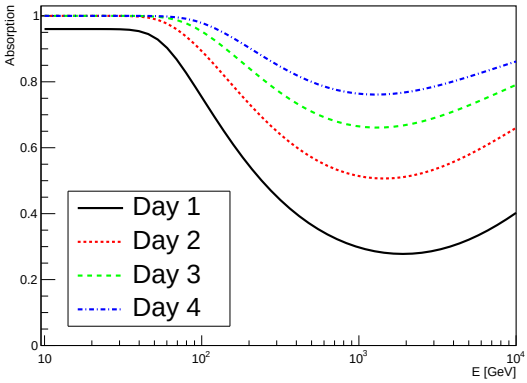

Fig. 11 Absorption of the gamma-ray emission on the radiation field of the photosphere and collision with it. Assumed parameters: $v_{sh} = 4500\,\mathrm{km\,s^{-1}}$, $R_{ph} = 200\,R_\odot$. Temperature of the photosphere is $T_{ph} = 10780\,\mathrm{K}$, $9490\,\mathrm{K}$, $8460\,\mathrm{K}$ and $7680\,\mathrm{K}$ for the time after the nova onset: 1 d (black solid), 2 d (red dotted), 3 d (green dashed), 4 d (blue dot-dashed) respectively.

time. Considering a period of recurrence of up to 10^5 years, the region over which this nova would dominate has a size of:

$$E_{\mathrm{dens,nova,recurrent}} = \frac{3E_{p,nova} \times 10^4}{4\pi R^3_{\mathrm{recurrent}}} \tag{17}$$

and the radius over which the protons accelerated by the nova would dominate over the energy density of the ISM would be $R_{\mathrm{recurrent}} \sim$13 pc.

C.3 Absorption of gamma-ray radiation

In both electron and proton models, the production of the gamma-ray radiation occurs relatively close to the photosphere $R_{sh} \approx 2.8(t/[\mathrm{day}]) \times R_{ph}$, a strong thermal source. We investigate the effect of absorption of the produced gamma rays on such a radiation field. We derive angle-dependent optical depths in vicinity of such thermal source and compute the average absorption as

$$\mathrm{Absorption}(E) = 0.5 \int_0^\pi e^{-\tau(E,\theta_{ph})} \sin\theta_{ph} \mathrm{d}\theta_{ph}, \tag{18}$$

where θ_{ph} is the angle between direction of photon and the radial direction from the center of the photosphere. Additionally we assume that photons crossing the photosphere are fully absorbed ($\tau = \infty$).

Derived absorption of the emission is presented in Fig. 11 for different days after the nova outburst. In general the absorption is not very strong, in particular at energies $\lesssim 300\,\mathrm{GeV}$, where gamma-ray emission was detected. Nevertheless it is taken into account in the modeling.

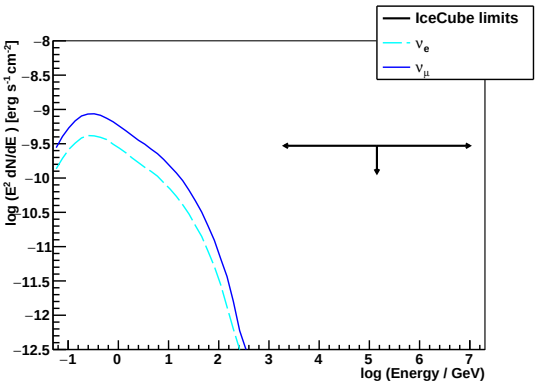

Fig. 12 Predicted neutrino emission (ν_e with cyan dashed line and ν_μ with solid blue line) associated to the proton model (see Fig. 3) compared with 90% C.L. limits obtained by the IceCube Collaboration [82].

C.4 Neutrino emission

The gamma-ray emission in hadronic scenario would be accompanied by neutrinos. We investigate the neutrino emission corresponding to the proton model presented in Fig. 3. In Fig. 12 we compare it with limits from the IceCube Collaboration [82]. It is clear that due to sub-TeV energies achieved by protons, these limits cannot constrain the model. We also investigated if SuperKamiokande could have detected neutrino emission associated to the nova outburst. However, due to low collection area at the GeV energies [83] the expected number of events is only of the order of 5×10^{-7}.

C.5 Day-by-day proton modeling

In addition to the modeling of an average state of the source in the first 4 days, we also perform modeling of individual days after the nova onset. The results of fits with the proton model are shown in left panels of Fig. 13. On individual days the preference of the proton model over the electron model is lower, however except for the first night, the electron model provides lower p value. Summing up over the four days χ^2 increases by 5.2 despite additional 4 parameters, results in ΔAIC= 13.2 which corresponds to AIC likelihood ratio of 1.4×10^{-3}.

Interestingly, the spectra show a hint of gradual softening of the power-law component accompanied by and increase of the value of the cut-off energy (see Fig. 14). Such behaviour is in line with the expectations from the cooling and acceleration time scales defined in Section C.1. Namely, due to low cooling losses of protons, their maximum energies are mainly determined by the duration of the acceleration. The dependence of the maximum energy of protons on time can be fit very well ($\chi^2/\mathrm{N_{dof}} = 0.54/3$) with such a scenario of proportional increase with time (corresponding to $\xi B = \mathrm{const}$). Such continuous increase of maximum proton energies could last until the shock is drained up from its energy, or is slowed down by the interstellar medium. However, as the target material dilutes with time, the expected gamma-ray emission would fall below the detectability level. Constant value of the cut energy can be excluded at chance probability 3.1×10^{-3} level ($\chi^2/\mathrm{N_{dof}} = 13.9/3$). It should be noted that while the fit only considers statistical uncertainties of the reconstructed maximum energy, it is unlikely that any systematic uncertainties would mimick such a gradient as the data are taken over a time span of only a few days in similar observational conditions.

C.6 Proton-lepton model

The presence of high-energy protons or electrons is not only dependent on their maximum energies (see Section C.1). Differences in the injection process of electrons and hadrons into the acceleration mechanism (see [84] and references therein) can cause preferential dominant acceleration of one or the other type of particles.

Following [13, 20], we test as well a model in which both electrons and protons are accelerated in the same shock. We assume injection with a power-law and exponential cut-off for both particles types. The cut-off energies are related by the cooling/acceleration balance (see Section C.1). The resulting best fit is presented in Fig. 15. The assumed spectral shape of injected electron and proton populations cannot explain the emission well ($\chi^2/\mathrm{N_{dof}} = 29.4/11$, corresponding to p-value of 2.0×10^{-3}). The best fit also requires $L_p/L_e \approx 2$, much larger than $\lesssim 0.1$ constrained in observations of V337 Del [13].

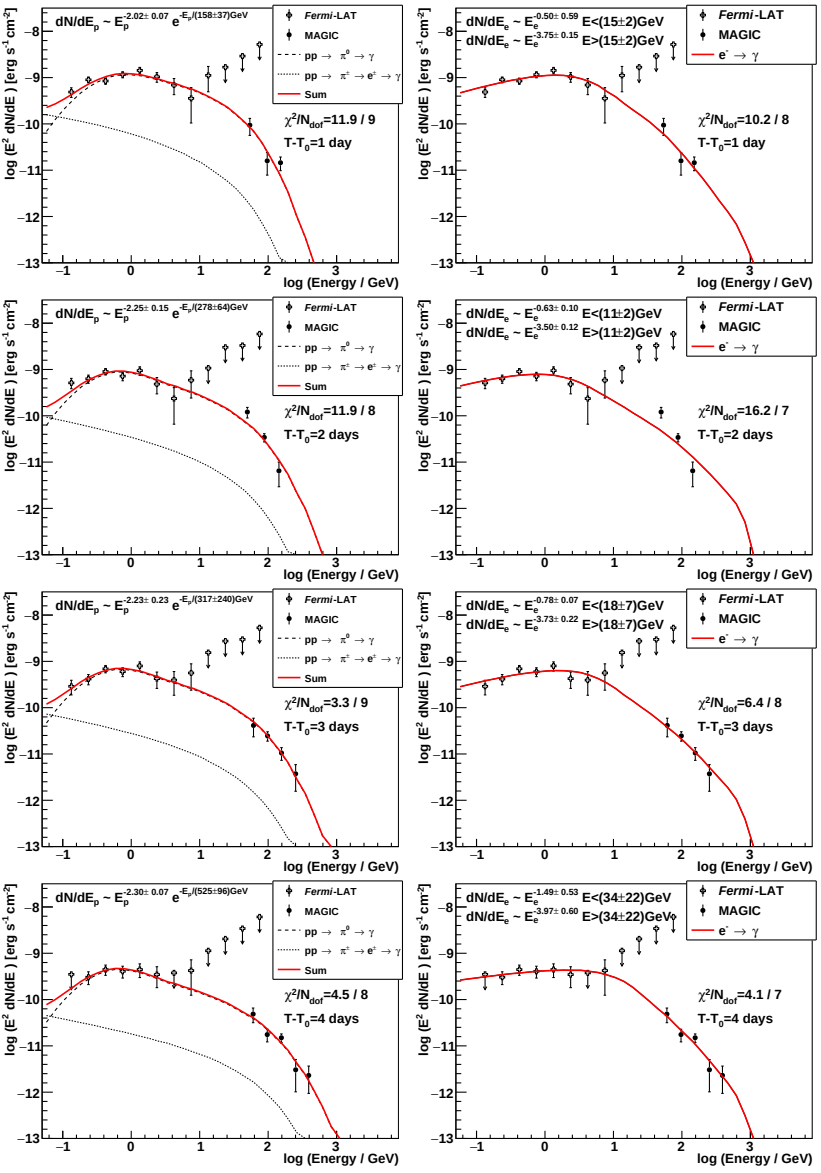

Fig. 13 Modeling of daily emission in proton model (left panels) and electron model (right panels) for first, second, third and fourth day after the nova eruption (from top to bottom). Individual line description as in Fig. 3.

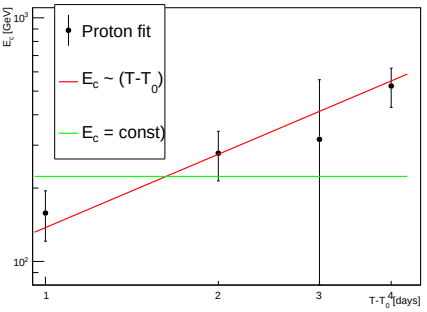

Fig. 14 The maximum energy of protons obtained from the theoretical model fits to the daily gamma-ray emission (points) shown in Fig. 13. Red and green line show, respectively, the scenario of proportional increase and constant value of maximum energy.

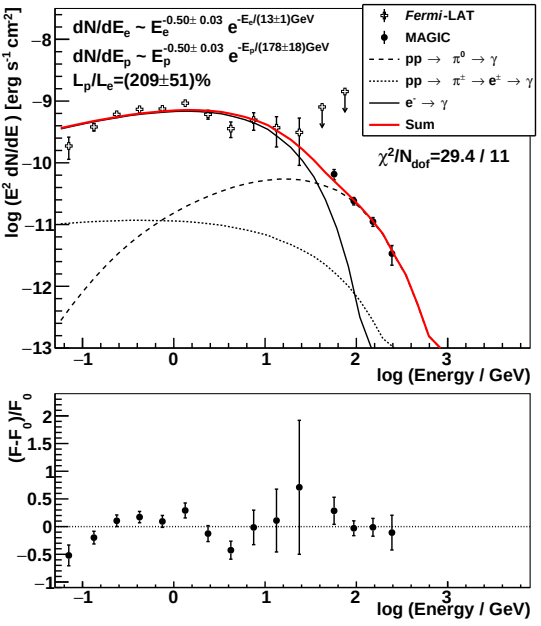

Fig. 15 Fit to the *Fermi*-LAT and MAGIC SED with a proton-electron model. Individual lines as in Fig. 3.

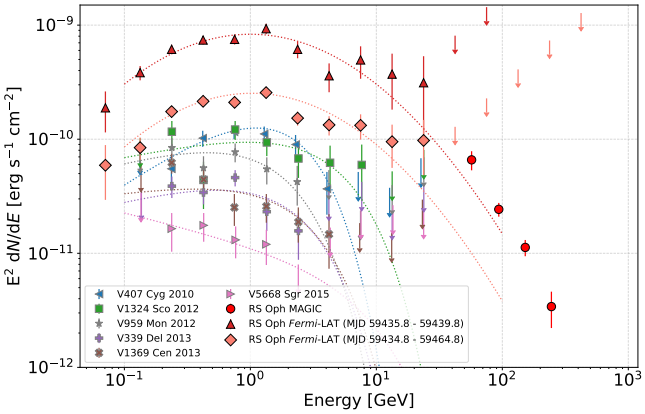

Fig. 16 Comparison of RS Oph to other *Fermi*-LAT-detected novae. Data taken from [10, 11, 85].

D RS Oph in context with other novae

D.1 Gamma-ray novae

To put the RS Oph eruption into context, we compared it to other published *Fermi*-LAT detections of novae: V407 Cyg 2010 [10], V3124 Sco 2012, V959 Mon 2012, V339 Del 2013 [11], V1369 Cen 2013 and V5668 Sgr 2015 [85]. There are other studies of *Fermi*-LAT novae [19], apart from several ATels and sub-threshold sources [86] of classical and symbiotic novae that are not included in the comparison presented in this section. It is important to mention that although RS Oph is considered to be a symbiotic nova, it was pointed out [87] that even though RNe have nova eruptions on symbiotic stars, they may not share all the properties of symbiotic novae (in particular very slow and low amplitude eruptions without Roche lobe overflow).

On Fig. 16, we present a comparison of the RS Oph *Fermi*-LAT SED coincident with the MAGIC detection (MJD 59435.8 - 59439.8) and the average of the full flare (MJD 59434.8 - 59464.8) compared to the aforementioned novae. We can see that both the flux corresponding to the simultaneous data, and the average flux during the whole eruption are from a factor of a few up to almost two orders of magnitude larger than previously-detected eruptions.

To perform meaningful comparisons, we defined the duration of RS Oph eruption the same way it has been done in [85]. With this definition, the duration is 30 days, that is comparable to the rest of the *Fermi*-LAT published novae. This has not only been the eruption with the highest flux, but also the most luminous one as it is shown in Fig. 17, for which we have used the results of the fit with an Exponential Cut-Off Power Law fit for E $>$ 0.1 GeV of the average flux from the eruption as in [85]. This statement is dependent on the assumed distance of 2.45 kpc (see the discussion in Section A.1).

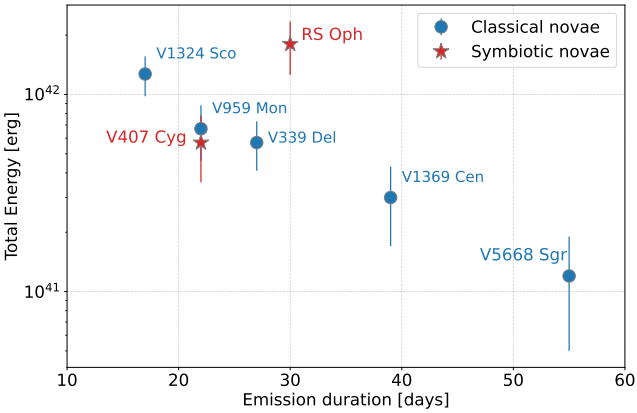

Fig. 17 Total energy vs duration of RS Oph 2021 outburst compared to that of the other novae detected by *Fermi*-LAT. Data taken from [10, 85].

In [85] there is the speculation that there is an apparent inverse relationship of the total energy with gamma-ray durations for classical novae, that would also roughly be followed by V407 Cyg. The fact that we measured that RS Oph has a factor of a few higher energy emitted in gamma rays, points to intrinsic differences between this eruption and the others detected in classical or symbiotic novae. The total power of gamma rays emitted from RS Oph, 1.8×10^{42} erg that is about $0.9 \times 10^{-2} (M_{ej}/(10^{-6} M_{sun})^{-1} (v_{sh}/4500\,\mathrm{km\,s^{-1}})^{-2} (d/2.45\,\mathrm{kpc})^2$ of the kinetic energy of the shock.

D.2 Detectability of novae at VHE gamma-ray range

We perform a comparison of the spectrum of RS Oph eruption with the most similar nova detected at gamma rays so far: V407 Cyg [10]. In the top panel of Fig. 18, we can see the comparison between the average V407 Cyg spectrum measured by *Fermi*-LAT during the 22 days of its eruption and the ULs by VERITAS [12] for a total of ∼5 hour observation time, compared to the MAGIC and the *Fermi*-LAT flux simultaneous to the MAGIC detection of RS Oph. We also scaled MAGIC and *Fermi*-LAT RS Oph flux to reach that of V407 Cyg measured by *Fermi*-LAT. We can see that in every case, the UL established by VERITAS on V407 Cyg lies above the extrapolation of the RS Oph flux measured by MAGIC, therefore the RS Oph results are in agreement with the non-detection by VERITAS, assuming that the VHE gamma-ray emission from V407 Cyg follows the same spectral shape as that of RS Oph.

There are physical differences between classical novae and RS Oph, a recurrent nova with a strong wind from the companion, that could cause the difference in gamma-ray emission. To evaluate the detectability of classical novae, we nevertheless performed a comparison between RS Oph and V339 Del [13], observed by MAGIC during its eruption. In the bottom panel of Fig. 18,

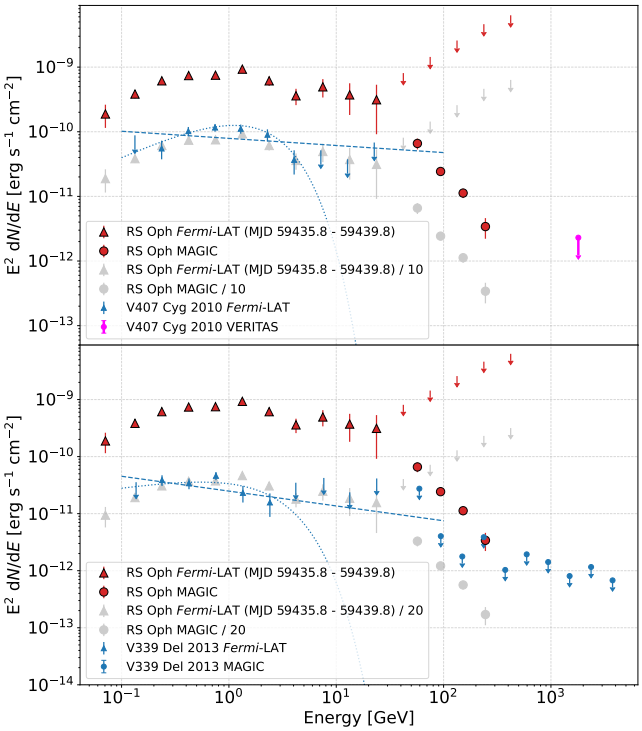

Fig. 18 Gamma-ray spectra of V407 Cyg (top panel) and V339 Del (bottom panel) compared to the measured (red) and scaled (gray) RS Oph gamma-ray spectra. Data taken from [10–13, 85].

we can see the average V339 Del spectrum measured by *Fermi*-LAT during the 27 days of the eruption and the MAGIC ULs compared to the RS Oph measurement of MAGIC and *Fermi*-LAT simultaneous to that of MAGIC. We also scaled the RS Oph flux to reach that of V339 Del measured by *Fermi*-LAT for the simultaneous data to MAGIC. We can see that the MAGIC ULs for V339 Del are below the RS Oph measurement, however, if we scale RS Oph flux down, the MAGIC ULs of V339 Del are above the MAGIC measurement of RS Oph. We note the caveat of comparing the average fluxes measured by *Fermi*-LAT for previous novae and that simultaneous to MAGIC measurement for RS Oph, in which the state was high.

We can conclude that the detection of RS Oph at VHE gamma rays was possible due to a higher gamma-ray flux, rather than favorable spectral distribution shape, and that other previously detected novae could have emitted

photons up to the same energies, that remained undetected due to the sensitivity of the observations. This means that a VHE gamma-ray instrument more sensitive in the ~ 100 GeV energies would open the possibility of detecting a large number of gamma-ray emitting novae if their emission extends up to VHE [22, 88].

References

[1] Bode, M.F., Evans, A.: Classical Novae vol. 43, (2008)

[2] Chomiuk, L., Metzger, B.D., Shen, K.J.: New insights into classical novae. Annual Review of Astronomy and Astrophysics **59**(1), 391–444 (2021) https://arxiv.org/abs/https://doi.org/10.1146/annurev-astro-112420-114502. https://doi.org/10.1146/annurev-astro-112420-114502

[3] Townsley, D.M., Bildsten, L.: Theoretical Modeling of the Thermal State of Accreting White Dwarfs Undergoing Classical Nova Cycles. *ApJ* **600**(1), 390–403 (2004) https://arxiv.org/abs/astro-ph/0306080 [astro-ph]. https://doi.org/10.1086/379647

[4] Mikołajewska, J.: Symbiotic Stars: Observations Confront Theory. Baltic Astronomy **21**, 5–12 (2012) https://arxiv.org/abs/1110.2361 [astro-ph.SR]. https://doi.org/10.1515/astro-2017-0352

[5] Ford, H.C.: The number of outbursts of a classical nova. *ApJ* **219**, 595 (1978). https://doi.org/10.1086/155819

[6] Schaefer, B.E.: Comprehensive Photometric Histories of All Known Galactic Recurrent Novae. *ApJS* **187**(2), 275–373 (2010) https://arxiv.org/abs/0912.4426 [astro-ph.SR]. https://doi.org/10.1088/0067-0049/187/2/275

[7] Webbink, R.F., Livio, M., Truran, J.W., Orio, M.: The Nature of the Recurrent Novae. *ApJ* **314**, 653 (1987). https://doi.org/10.1086/165095

[8] Mikolajewska, J.: The Place of Recurrent Novae Among the Symbiotic Stars. In: Evans, A., Bode, M.F., O'Brien, T.J., Darnley, M.J. (eds.) RS Ophiuchi (2006) and the Recurrent Nova Phenomenon. Astronomical Society of the Pacific Conference Series, vol. 401, p. 42 (2008)

[9] Chen, W., Shrader, C.R., Livio, M.: The Properties of X-Ray and Optical Light Curves of X-Ray Novae. *ApJ* **491**(1), 312–338 (1997) https://arxiv.org/abs/astro-ph/9707138 [astro-ph]. https://doi.org/10.1086/304921

[10] Abdo, A.A., et al.: Gamma-Ray Emission Concurrent with the Nova in the Symbiotic Binary V407 Cygni. Science **329**(5993), 817–821 (2010) https://arxiv.org/abs/1008.3912 [astro-ph.HE]. https://doi.org/10.1126/

science.1192537

[11] Ackermann, M., et al.: Fermi establishes classical novae as a distinct class of gamma-ray sources. Science **345**(6196), 554–558 (2014) https://arxiv.org/abs/1408.0735 [astro-ph.HE]. https://doi.org/10.1126/science.1253947

[12] Aliu, E., et al.: VERITAS Observations of the Nova in V407 Cygni. *ApJ* **754**(1), 77 (2012) https://arxiv.org/abs/1205.5287 [astro-ph.HE]. https://doi.org/10.1088/0004-637X/754/1/77

[13] Ahnen, M.L., et al.: Very high-energy γ-ray observations of novae and dwarf novae with the MAGIC telescopes. *A&A* **582**, 67 (2015) https://arxiv.org/abs/1508.04902 [astro-ph.HE]. https://doi.org/10.1051/0004-6361/201526478

[14] Dobrzycka, D., Kenyon, S.J.: A New Spectroscopic Orbit for RS Ophiuchi. *AJ* **108**, 2259 (1994). https://doi.org/10.1086/117238

[15] Geary, K.: Outburst of RS Ophiuchi. vsnet-alert **26131** (2021)

[16] Cheung, C.C., Ciprini, S., Johnson, T.J.: Fermi-LAT Gamma-ray Detection of the Recurrent Nova RS Oph. The Astronomer's Telegram **14834**, 1 (2021)

[17] Wagner, S.J., H. E. S. S. Collaboration: Detection of VHE gamma-ray emission from the recurrent nova RS Ophiuchi with H.E.S.S. The Astronomer's Telegram **14844**, 1 (2021)

[18] Martin, P., Dubus, G., Jean, P., Tatischeff, V., Dosne, C.: Gamma-ray emission from internal shocks in novae. *A&A* **612**, 38 (2018) https://arxiv.org/abs/1710.05515 [astro-ph.HE]. https://doi.org/10.1051/0004-6361/201731692

[19] Aydi, E., et al.: Direct evidence for shock-powered optical emission in a nova. Nature Astronomy **4**, 776–780 (2020) https://arxiv.org/abs/2004.05562 [astro-ph.HE]. https://doi.org/10.1038/s41550-020-1070-y

[20] Sitarek, J., Bednarek, W.: GeV-TeV gamma rays and neutrinos from the Nova V407 Cygni. *Phys. Rev. D* **86**(6), 063011 (2012) https://arxiv.org/abs/1208.6200 [astro-ph.HE]. https://doi.org/10.1103/PhysRevD.86.063011

[21] Akaike, H.: A New Look at the Statistical Model Identification. IEEE Transactions on Automatic Control **19**, 716–723 (1974)

[22] Metzger, B.D., Caprioli, D., Vurm, I., Beloborodov, A.M., Bartos,

I., Vlasov, A.: Novae as Tevatrons: prospects for CTA and IceCube. *MNRAS* **457**(2), 1786–1795 (2016) https://arxiv.org/abs/1510.07639 [astro-ph.HE]. https://doi.org/10.1093/mnras/stw123

[23] Bath, G.T., Shaviv, G.: The space density, recurrence rate and classification of novae. *MNRAS* **183**, 515–522 (1978). https://doi.org/10.1093/mnras/183.3.515

[24] Mikołajewska, J., Shara, M.M.: The Massive CO White Dwarf in the Symbiotic Recurrent Nova RS Ophiuchi. *ApJ* **847**(2), 99 (2017) https://arxiv.org/abs/1702.08732 [astro-ph.SR]. https://doi.org/10.3847/1538-4357/aa87b6

[25] Anupama, G.C., Mikołajewska, J.: Recurrent novae at quiescence: systems with giant secondaries. *A&A* **344**, 177–187 (1999) https://arxiv.org/abs/astro-ph/9812432 [astro-ph]

[26] Tatischeff, V., Hernanz, M.: Evidence for Nonlinear Diffusive Shock Acceleration of Cosmic Rays in the 2006 Outburst of the Recurrent Nova RS Ophiuchi. *ApJ* **663**(2), 101–104 (2007) https://arxiv.org/abs/0705.4422 [astro-ph]. https://doi.org/10.1086/520049

[27] Brandi, E., Quiroga, C., Mikołajewska, J., Ferrer, O.E., García, L.G.: Spectroscopic orbits and variations of RS Ophiuchi. *A&A* **497**(3), 815–825 (2009) https://arxiv.org/abs/0902.2177 [astro-ph.SR]. https://doi.org/10.1051/0004-6361/200811417

[28] Fekel, F.C., Joyce, R.R., Hinkle, K.H., Skrutskie, M.F.: Infrared Spectroscopy of Symbiotic Stars. I. Orbits for Well-Known S-Type Systems. *AJ* **119**(3), 1375–1388 (2000). https://doi.org/10.1086/301260

[29] Schaefer, B.E.: Orbital Periods for Three Recurrent Novae. *ApJ* **697**(1), 721–729 (2009) https://arxiv.org/abs/0903.1349 [astro-ph.SR]. https://doi.org/10.1088/0004-637X/697/1/721

[30] Iijima, T.: Circumstellar Envelope of RS Ophiuchi. In: Evans, A., Bode, M.F., O'Brien, T.J., Darnley, M.J. (eds.) RS Ophiuchi (2006) and the Recurrent Nova Phenomenon. Astronomical Society of the Pacific Conference Series, vol. 401, p. 115 (2008)

[31] Munari, U., Valisa, P.: Echelle spectroscopy of RS Oph at day +0.87 from optical discovery. The Astronomer's Telegram **14840**, 1 (2021)

[32] Mikolajewska, J., Aydi, E., Buckley, D., Galan, C., Orio, M.: SALT high resolution spectroscopy of RS Oph: evidence for acceleration of the nova ejecta. The Astronomer's Telegram **14852**, 1 (2021)

[33] Rupen, M.P., Mioduszewski, A.J., Sokoloski, J.L.: An Expanding Shell and Synchrotron Jet in RS Ophiuchi. *ApJ* **688**(1), 559–567 (2008) https://arxiv.org/abs/0711.1142 [astro-ph]. https://doi.org/10.1086/525555

[34] Bode, M.F., Kahn, F.D.: A model for the outburst of nova RS Ophiuchi in 1985. *MNRAS* **217**, 205–215 (1985). https://doi.org/10.1093/mnras/217.1.205

[35] Linford, J.D., et al.: The Peculiar Multiwavelength Evolution Of V1535 Sco. *ApJ* **842**(2), 73 (2017) https://arxiv.org/abs/1703.03333 [astro-ph.HE]. https://doi.org/10.3847/1538-4357/aa7512

[36] Kantharia, N.G., et al.: Insights into the evolution of symbiotic recurrent novae from radio synchrotron emission: V745 Scorpii and RS Ophiuchi. *MNRAS* **456**(1), 49–53 (2016) https://arxiv.org/abs/1510.02203 [astro-ph.HE]. https://doi.org/10.1093/mnrasl/slv154

[37] Hjellming, R.M., van Gorkom, J.H., Taylor, A.R., Sequist, E.R., Padin, S., Davis, R.J., Bode, M.F.: Radio Observations of the 1985 Outburst of RS Ophiuchi. *ApJ* **305**, 71 (1986). https://doi.org/10.1086/184687

[38] Bode, M.F.: RS Ophiuchi (1985) and the Recurrent Nova Phenomenon. Proceedings of the Manchester Conference, Held at Manchester, UK, 16 - 18 December 1985., (1987)

[39] Barry, R.K., Mukai, K., Sokoloski, J.L., Danchi, W.C., Hachisu, I., Evans, A., Gehrz, R., Mikolajewska, J.: On the Distance of RS Ophiuchi. In: Evans, A., Bode, M.F., O'Brien, T.J., Darnley, M.J. (eds.) RS Ophiuchi (2006) and the Recurrent Nova Phenomenon. Astronomical Society of the Pacific Conference Series, vol. 401, p. 52 (2008)

[40] Schaefer, B.E.: The distances to Novae as seen by Gaia. *MNRAS* **481**(3), 3033–3051 (2018) https://arxiv.org/abs/1809.00180 [astro-ph.SR]. https://doi.org/10.1093/mnras/sty2388

[41] Gaia Collaboration, et al.: Gaia Early Data Release 3. Summary of the contents and survey properties. *A&A* **649**, 1 (2021) https://arxiv.org/abs/2012.01533 [astro-ph.GA]. https://doi.org/10.1051/0004-6361/202039657

[42] Rupen, M.P., Mioduszewski, A.J., Sokoloski, J.L.: An expanding shell and synchrotron jet in RS ophiuchi. The Astrophysical Journal **688**(1), 559–567 (2008). https://doi.org/10.1086/525555

[43] Gaia Collaboration, et al.: Gaia Data Release 2. Summary of the contents and survey properties. *A&A* **616**, 1 (2018) https://arxiv.org/abs/1804.09365 [astro-ph.GA]. https://doi.org/10.1051/0004-6361/201833051

[44] Aleksić, J., et al.: The major upgrade of the MAGIC telescopes, Part I: The hardware improvements and the commissioning of the system. Astroparticle Physics **72**, 61–75 (2016) https://arxiv.org/abs/1409.6073 [astro-ph.IM]. https://doi.org/10.1016/j.astropartphys.2015.04.004

[45] Aleksić, J., et al.: The major upgrade of the MAGIC telescopes, Part II: A performance study using observations of the Crab Nebula. Astroparticle Physics **72**, 76–94 (2016) https://arxiv.org/abs/1409.5594 [astro-ph.IM]. https://doi.org/10.1016/j.astropartphys.2015.02.005

[46] Zanin, R., Carmona, E., J., S., P., C., K., F., M., G., S., L., M., L., A., M., for the MAGIC collaboration: MARS, the MAGIC analysis and reconstruction software . In: Proc. of the 33th International Cosmic Ray Conference (ICRC), p. 773 (2013). https://doi.org/http://inspirehep.net/record/1412925/files/icrc2013-0773.pdf

[47] MAGIC Collaboration, et al.: VHE gamma-ray detection of FSRQ QSO B1420+326 and modeling of its enhanced broadband state in 2020. *A&A* **647**, 163 (2021) https://arxiv.org/abs/2012.11380 [astro-ph.HE]. https://doi.org/10.1051/0004-6361/202039687

[48] Atwood, W.B., et al.: The Large Area Telescope on the Fermi Gamma-Ray Space Telescope Mission. *ApJ* **697**(2), 1071–1102 (2009) https://arxiv.org/abs/0902.1089 [astro-ph.IM]. https://doi.org/10.1088/0004-637X/697/2/1071

[49] Wood, M., Caputo, R., Charles, E., Di Mauro, M., Magill, J., Perkins, J.S., Fermi-LAT Collaboration: Fermipy: An open-source Python package for analysis of Fermi-LAT Data. In: 35th International Cosmic Ray Conference (ICRC2017). International Cosmic Ray Conference, vol. 301, p. 824 (2017)

[50] Abdollahi, S., et al.: Fermi large area telescope fourth source catalog. The Astrophysical Journal Supplement Series **247**(1), 33 (2020). https://doi.org/10.3847/1538-4365/ab6bcb

[51] Ballet, J., Burnett, T.H., Digel, S.W., Lott, B.: Fermi Large Area Telescope Fourth Source Catalog Data Release 2. arXiv e-prints, 2005–11208 (2020) https://arxiv.org/abs/2005.11208 [astro-ph.HE]

[52] Mattox, J.R., et al.: The Likelihood Analysis of EGRET Data. *ApJ* **461**, 396 (1996). https://doi.org/10.1086/177068

[53] Nilsson, K., et al.: Long-term optical monitoring of TeV emitting blazars. I. Data analysis. *A&A* **620**, 185 (2018) https://arxiv.org/abs/1810.01751 [astro-ph.HE]. https://doi.org/10.1051/0004-6361/201833621

[54] Munari, U., et al.: The ANS Collaboration Monitoring Program. Baltic Astronomy **21**, 13–21 (2012). https://doi.org/10.1515/astro-2017-0353

[55] Munari, U., Moretti, S.: Characterizing the Photometric Response of the ANS Collaboration Monitoring Program. Baltic Astronomy **21**, 22–31 (2012). https://doi.org/10.1515/astro-2017-0354

[56] Henden, A.A., Levine, S.E., Terrell, D., Smith, T.C., Welch, D.: Data Release 3 of the AAVSO All-Sky Photometric Survey (APASS). JAAVSO **40**(1), 430 (2012)

[57] Henden, A., Munari, U.: The APASS all-sky, multi-epoch BVgri photometric survey. Contributions of the Astronomical Observatory Skalnate Pleso **43**(3), 518–522 (2014)

[58] Landolt, A.U.: UBVRI Photometric Standard Stars Around the Celestial Equator: Updates and Additions. *AJ* **137**(5), 4186–4269 (2009) https://arxiv.org/abs/0904.0638 [astro-ph.SR]. https://doi.org/10.1088/0004-6256/137/5/4186

[59] Munari, U., Henden, A., Frigo, A., Dallaporta, S.: APASS discovery and characterization of 180 variable stars in Aquarius. Journal of Astronomical Data **20**, 4 (2014)

[60] Munari, U., et al.: APASS Landolt-Sloan BVgri Photometry of RAVE Stars. I. Data, Effective Temperatures, and Reddenings. *AJ* **148**(5), 81 (2014) https://arxiv.org/abs/1408.5476 [astro-ph.SR]. https://doi.org/10.1088/0004-6256/148/5/81

[61] Munari, U., et al.: The 2006 Outburst of the Recurrent Nova RS OPH. Baltic Astronomy **16**, 46–48 (2007)

[62] Teyssier, F.: Eruptive stars monitoring and the ARAS database. Contributions of the Astronomical Observatory Skalnate Pleso **49**(2), 217–227 (2019)

[63] Hachisu, I., Kato, M.: The UBV Color Evolution of Classical Novae. I. Nova-giant Sequence in the Color-Color Diagram. *ApJ* **785**(2), 97 (2014) https://arxiv.org/abs/1401.7113 [astro-ph.SR]. https://doi.org/10.1088/0004-637X/785/2/97

[64] Cardelli, J.A., Clayton, G.C., Mathis, J.S.: The Relationship between Infrared, Optical, and Ultraviolet Extinction. *ApJ* **345**, 245 (1989). https://doi.org/10.1086/167900

[65] Bessell, M.S., Castelli, F., Plez, B.: Model atmospheres broad-band colors, bolometric corrections and temperature calibrations for O - M stars. *A&A*

333, 231–250 (1998)

[66] Skopal, A.: Multiwavelength modeling the SED of supersoft X-ray sources. II. RS Ophiuchi: From the explosion to the SSS phase. *New A* **36**, 128–138 (2015) https://arxiv.org/abs/1402.6126 [astro-ph.SR]. https://doi.org/10.1016/j.newast.2013.12.005

[67] Munari, U., Valisa, P.: The 2021 outburst of RS Oph. A pictorial atlas of the spectroscopic evolution: the first 18 days. arXiv e-prints, 2109–01101 (2021) https://arxiv.org/abs/2109.01101 [astro-ph.SR]

[68] Leone, F., et al.: A Method to Calibrate the High-resolution Catania Astrophysical Observatory Spectropolarimeter. *AJ* **151**(5), 116 (2016). https://doi.org/10.3847/0004-6256/151/5/116

[69] Cosentino, R., et al.: Harps-N: the new planet hunter at TNG. In: McLean, I.S., Ramsay, S.K., Takami, H. (eds.) Ground-based and Airborne Instrumentation for Astronomy IV. Society of Photo-Optical Instrumentation Engineers (SPIE) Conference Series, vol. 8446, p. 84461 (2012). https://doi.org/10.1117/12.925738

[70] Catanzaro, G., et al.: CAOS spectroscopy of Am stars Kepler targets. *MNRAS* **451**(1), 184–195 (2015) https://arxiv.org/abs/1504.07740 [astro-ph.SR]. https://doi.org/10.1093/mnras/stv952

[71] Skopal, A., Pribulla, T., Buil, C., Vittone, A., Errico, L.: Non-spherical Mass Outflow from RS Ophiuchi During its 2006 Outburst. In: Evans, A., Bode, M.F., O'Brien, T.J., Darnley, M.J. (eds.) RS Ophiuchi (2006) and the Recurrent Nova Phenomenon. Astronomical Society of the Pacific Conference Series, vol. 401, p. 227 (2008)

[72] Mondal, A., Anupama, G.C., Kamath, U.S., Das, R., Selvakumar, G., Mondal, S.: Optical spectroscopy of the recurrent nova RS Ophiuchi - from the outburst of 2006 to quiescence. *MNRAS* **474**(3), 4211–4224 (2018) https://arxiv.org/abs/1711.07643 [astro-ph.SR]. https://doi.org/10.1093/mnras/stx2988

[73] Ribeiro, V.A.R.M., et al.: The Expanding Nebular Remnant of the Recurrent Nova RS Ophiuchi (2006). II. Modeling of Combined Hubble Space Telescope Imaging and Ground-based Spectroscopy. *ApJ* **703**(2), 1955–1963 (2009) https://arxiv.org/abs/0908.2704 [astro-ph.SR]. https://doi.org/10.1088/0004-637X/703/2/1955

[74] Sokoloski, J.L., Rupen, M.P., Mioduszewski, A.J.: Uncovering the Nature of Nova Jets: A Radio Image of Highly Collimated Outflows from RS Ophiuchi. *ApJ* **685**(2), 137 (2008). https://doi.org/10.1086/592602

[75] Bode, M.F., Harman, D.J., O'Brien, T.J., Bond, H.E., Starrfield, S., Darnley, M.J., Evans, A., Eyres, S.P.S.: Hubble Space Telescope Imaging of the Expanding Nebular Remnant of the 2006 Outburst of the Recurrent Nova RS Ophiuchi. *ApJ* **665**(1), 63–66 (2007) https://arxiv.org/abs/0706.2745 [astro-ph]. https://doi.org/10.1086/520929

[76] Leone, F., et al.: The solar-like 'Second Spectrum' and polarized metal lines in the emission of the post-AGB binary 89 Herculis. *MNRAS* **480**(2), 1656–1665 (2018) https://arxiv.org/abs/1804.08255 [astro-ph.SR]. https://doi.org/10.1093/mnras/sty1882

[77] Leone, F., et al.: A Method to Measure the Transverse Magnetic Field and Orient the Rotational Axis of Stars. *ApJ* **848**(2), 107 (2017) https://arxiv.org/abs/1704.03376 [astro-ph.SR]. https://doi.org/10.3847/1538-4357/aa8d72

[78] Moderski, R., Sikora, M., Coppi, P.S., Aharonian, F.: Klein-Nishina effects in the spectra of non-thermal sources immersed in external radiation fields. *MNRAS* **363**(3), 954–966 (2005) https://arxiv.org/abs/astro-ph/0504388 [astro-ph]. https://doi.org/10.1111/j.1365-2966.2005.09494.x

[79] Shafter, A.W.: The Galactic Nova Rate Revisited. *ApJ* **834**(2), 196 (2017) https://arxiv.org/abs/1606.02358 [astro-ph.SR]. https://doi.org/10.3847/1538-4357/834/2/196

[80] Walch, S., Naab, T.: The energy and momentum input of supernova explosions in structured and ionized molecular clouds. *MNRAS* **451**(3), 2757–2771 (2015) https://arxiv.org/abs/1410.0011 [astro-ph.GA]. https://doi.org/10.1093/mnras/stv1155

[81] Rozwadowska, K., Vissani, F., Cappellaro, E.: On the rate of core collapse supernovae in the milky way. *New A* **83**, 101498 (2021) https://arxiv.org/abs/2009.03438 [astro-ph.HE]. https://doi.org/10.1016/j.newast.2020.101498

[82] Pizzuto, A., Vandenbroucke, J., Santander, M., IceCube Collaboration: Nova RS Oph: upper limits from a search for coincident neutrinos with IceCube. The Astronomer's Telegram **14851**, 1 (2021)

[83] Collaboration, T.S.-K.: Search for neutrinos in coincidence with gravitational wave events from the LIGO-Virgo O3a Observing Run with the Super-Kamiokande detector - Data release. Zenodo. For the Super-Kamiokande collaboration (2021). https://doi.org/10.5281/zenodo.4724823. https://doi.org/10.5281/zenodo.4724823

[84] Arbutina, B., Zeković, V.: Non-linear diffusive shock acceleration: A recipe for injection of electrons. Astroparticle Physics **127**, 102546

(2021) https://arxiv.org/abs/2012.15117 [astro-ph.HE]. https://doi.org/10.1016/j.astropartphys.2020.102546

[85] Cheung, C.C., et al.: Fermi-LAT Gamma-Ray Detections of Classical Novae V1369 Centauri 2013 and V5668 Sagittarii 2015. *ApJ* **826**(2), 142 (2016) https://arxiv.org/abs/1605.04216 [astro-ph.HE]. https://doi.org/10.3847/0004-637X/826/2/142

[86] Franckowiak, A., Jean, P., Wood, M., Cheung, C.C., Buson, S.: Search for gamma-ray emission from Galactic novae with the Fermi-LAT. *A&A* **609**, 120 (2018) https://arxiv.org/abs/1710.04736 [astro-ph.HE]. https://doi.org/10.1051/0004-6361/201731516

[87] Strope, R.J., Schaefer, B.E., Henden, A.A.: CATALOG OF 93 NOVA LIGHT CURVES: CLASSIFICATION AND PROPERTIES. The Astronomical Journal **140**(1), 34–62 (2010). https://doi.org/10.1088/0004-6256/140/1/34

[88] Cherenkov Telescope Array Consortium, et al.: Science with the Cherenkov Telescope Array, (2019). https://doi.org/10.1142/10986